

Advances in Deep Concealed Scene Understanding

Deng-Ping Fan, Ge-Peng Ji, Peng Xu, Ming-Ming Cheng, Christos Sakaridis, Luc Van Gool

Abstract—Concealed scene understanding (CSU) is a hot computer vision topic aiming to perceive objects with camouflaged properties. The current boom in its advanced techniques and novel applications make it timely to provide an up-to-date survey to enable researchers to understand the global picture of the CSU field, including both current achievements and major challenges. This paper makes four contributions: (1) For the first time, we present a comprehensive survey of the deep learning techniques oriented at CSU, including a background with its taxonomy, task-unique challenges, and a review of its developments in the deep learning era via surveying existing datasets and deep techniques. (2) For a quantitative comparison of the state-of-the-art, we contribute the largest and latest benchmark for Concealed Object Segmentation (COS). (3) To evaluate the transferability of deep CSU in practical scenarios, we re-organize the largest concealed defect segmentation dataset termed CDS2K with the hard cases from diversified industrial scenarios, on which we construct a comprehensive benchmark. (4) We discuss open problems and potential research directions for this community. Our code and datasets are available at <https://github.com/DengPingFan/CSU>, which will be updated continuously to watch and summarize the advancements in this rapidly evolving field.

Index Terms—Concealed Scene Understanding, Segmentation, Detection, Survey, Introductory, Taxonomy, Deep Learning.



1 INTRODUCTION

CONCEALED scene understanding (CSU) aims to recognize objects with camouflaged properties in natural or artificial scenarios. Due to its visual complexity, CSU is a challenging problem compared with conventional scene understanding tasks such as recognizing salient [1] or general [2] objects. It has numerous real-world applications, including computer vision (*e.g.*, for search-and-rescue work or rare species discovery), healthcare (*e.g.*, automatic diagnosis for colorectal polyp [3] and lung lesion [4]), agriculture (*e.g.*, pest [5] and fruit ripeness [6] detection), content creation (*e.g.*, recreational art [7]), *etc*. In the past decade, both academics and industry have widely studied CSU, and various camouflaged cases have been systematically explored by traditional computer vision and pattern recognition techniques, including hand-engineered patterns (*e.g.*, motion cues [8], [9], optical flow [10], [11]), heuristic priors (*e.g.*, color [12], texture [13], intensity [14], [15]) and combination techniques [16], [17], [18].

In recent years, thanks to both several self-contained benchmarks (*e.g.*, COD10K [19], [22] and NC4K [23]) and the rapid development of deep learning, this field has been advanced further. In 2020, Fan *et al.* [19] released the first large-scale public dataset COD10K that has advanced the development of visual perception tasks, especially in concealed scenarios. This has also inspired other related disciplines. For instance, psychologist Michael W. Eysenck [24] studied the cooperative relationship between AI and human cognition. Mei *et al.* [25], [26] proposed a distraction-aware framework for segmenting camouflaged objects,

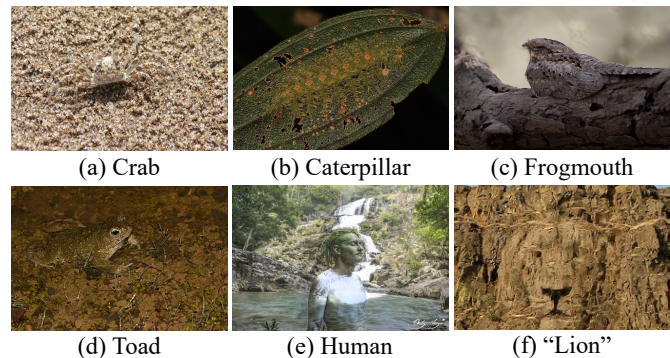


Fig. 1. **Sample gallery of concealed scenarios.** (a-d) show natural animals selected from [19]. (e) depicts a concealed human in art from [20]. (f) features a synthesized “lion” by [21].

which can also be extended to identifying transparent materials in natural scenes [27]. In 2023, Ji *et al.* [28] developed an efficient model that learns textures from object-level gradients, and its transferability has been verified in various downstream applications, *e.g.*, polyp segmentation and road crack detection.

However, to our knowledge, the CSU tasks are relatively separately discussed in general and their model generalization from academic settings to industrial scenarios is understudied. Given the current boom in their advanced deep techniques and novel applications, this calls for an up-to-date survey to enable researchers to capture the global landscape of the CSU field, including both current achievements and major challenges. Thus, in this paper, we mainly review the state and recent deep learning-based advances of CSU. Meanwhile, we contribute a large-scale concealed defect segmentation dataset termed CDS2K with the hard cases from diversified industrial scenarios. We construct a comprehensive benchmark to explore the potential from academic research to industrial applications of the CSU community.

- Deng-Ping Fan, Christos Sakaridis, and Luc Van Gool are with the Computer Vision Lab (CVL), ETH Zurich, Zurich, Switzerland.
- Ge-Peng Ji is with the College of Engineering, Computing & Cybernetics, ANU, Canberra, Australia.
- Peng Xu is with the Department of Electronic Engineering, Tsinghua University, Beijing, China.
- Ming-Ming Cheng is with the Nankai University, Tianjin, China.

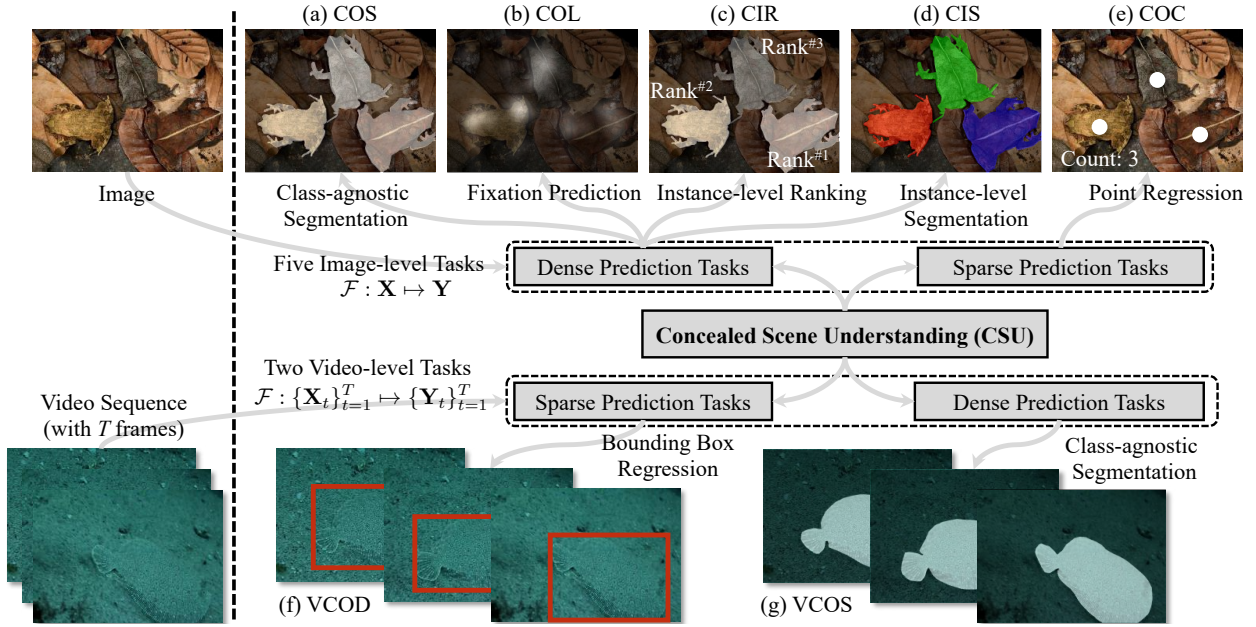


Fig. 2. **A taxonomy of seven popular CSU tasks.** This taxonomy categorizes seven popular tasks in CSU. Five of these are image-level tasks: (a) concealed object segmentation (COS), (b) concealed object localization (COL), (c) concealed instance ranking (CIR), (d) concealed instance segmentation (CIS), and (e) concealed object counting (COC). The remaining two are video-level tasks: (f) video concealed object segmentation (VCOS) and (g) video concealed object detection (VCOD). Each task has its own corresponding annotation visualization, which is explained in detail in §2.1.

Previous Surveys and Scope. To our knowledge, only a few survey papers were published in the CSU community, which [29], [30] mainly review non-deep techniques. There are some benchmarks [31], [32] with narrow scopes, such as image-level segmentation, where only a few deep methods were evaluated. In this paper, we present a comprehensive survey of the deep learning techniques oriented at CSU, forming a larger landscape, and contribute more extensive benchmarks with more comprehensive comparison and practical application-oriented evaluation.

Contributions. Our contributions are summarized as follows: (1) We represent the initial effort to examine deep learning techniques tailored towards CSU thoroughly. This includes an overview of its classification and specific obstacles, as well as an assessment of its advancements during the era of deep learning, achieved through an examination of existing datasets and techniques. (2) To provide a quantitative evaluation of the current state-of-the-art, we have created a new benchmark for Concealed Object Segmentation (COS), which is a crucial and highly successful area within CSU. This benchmark is the most up-to-date and comprehensive available. (3) To assess the applicability of deep CSU in real-world scenarios, we have restructured the CDS2K dataset – the largest dataset for concealed defect segmentation – to include challenging cases from various industrial settings. We have utilized this updated dataset to create a comprehensive benchmark for evaluation. (4) Our discussion delves into the present obstacles, available prospects, and prospective research areas for the CSU community.

2 BACKGROUND

2.1 Task Taxonomy and Formulation

2.1.1 Image-level CSU

In this section, we introduce five commonly used image-level CSU tasks, which can be formulated as a mapping function $F: \mathbf{X} \mapsto \mathbf{Y}$

that converts the input space \mathbf{X} into the target space \mathbf{Y} .

- **Concealed Object Segmentation (COS)** [22], [28] is a class-agnostic dense prediction task, segmenting concealed regions or objects with unknown categories. As presented in Fig. 2 (a), the model $F_{\text{COS}}: \mathbf{X} \mapsto \mathbf{Y}$ is supervised by a binary mask \mathbf{Y} to predict a probability $\mathbf{p} \in [0, 1]$ for each pixel \mathbf{x} of image \mathbf{X} , which is the confidence level that the model determines whether \mathbf{x} belongs to the concealed region.

- **Concealed Object Localization (COL)** [23], [33] aims to identify the most noticeable region of concealed objects, which is in line with human perception psychology [33]. This task is to learn a dense mapping $F_{\text{COL}}: \mathbf{X} \mapsto \mathbf{Y}$. The output \mathbf{Y} is a non-binary fixation map captured by an eye tracker device, as illustrated in Fig. 2 (b). Essentially, the probability prediction $\mathbf{p} \in [0, 1]$ for a pixel \mathbf{x} indicates how conspicuous its camouflage is.

- **Concealed Instance Ranking (CIR)** [23], [33] is to rank different instances in a concealed scene based on their detectability. The level of camouflage is used as the basis for this ranking. The objective of the CIR task is to learn a dense mapping $F_{\text{CIR}}: \mathbf{X} \mapsto \mathbf{Y}$ between the input space \mathbf{X} and the camouflage ranking space \mathbf{Y} , where \mathbf{Y} represents per-pixel annotations for each instance with corresponding rank levels. For example, in Fig. 2 (c), there are three toads with different camouflage levels, and their ranking labels are from [23]. To perform this task, one can replace the category ID for each instance with rank labels in instance segmentation models like Mask R-CNN [34].

- **Concealed Instance Segmentation (CIS)** [35], [36] is a technique that aims to identify instances in concealed scenarios based on their semantic characteristics. Unlike general instance segmentation [37], [38], where each instance is assigned a category label, CIS recognizes the attributes of concealed objects to distinguish between different entities more effectively. To achieve this, CIS

employs a mapping function $F_{\text{CIS}} : \mathbf{X} \mapsto \mathbf{Y}$, where \mathbf{Y} is a scalar set comprising various entities used to parse each pixel. This concept is illustrated in Fig. 2 (d).

Concealed Object Counting (COC) [39] is a newly emerging topic in CSU that aims to estimate the number of instances concealed within their surroundings. As illustrated in Fig. 2 (e), the COC is to estimate center coordinates for each instance and generate their counts. Its formulation can be defined as $F_{\text{COC}} : \mathbf{X} \mapsto \mathbf{Y}$, where \mathbf{X} is the input image and \mathbf{Y} represents the output density map that indicates the concealed instances in scenes.

Overall, the image-level CSU tasks can be categorized into two groups based on their semantics: object-level (COS and COL) and instance-level (CIR, COC, and CIS). Object-level tasks focus on perceiving objects while instance-level ones aim to recognize semantics to distinguish different entities. Additionally, COC is regarded as a sparse prediction task based on its output form, whereas the others belong to dense prediction tasks. Among the literature reviewed in Table 1, COS has been extensively researched while research on the other three tasks is gradually increasing.

2.1.2 Video-level CSU

Given a video clip $\{\mathbf{X}_t\}_{t=1}^T$ containing T concealed frames, video-level CSU can be formulated as a mapping function $F : \{\mathbf{X}_t\}_{t=1}^T \mapsto \{\mathbf{Y}_t\}_{t=1}^T$ for parsing dense spatial-temporal correspondences, where \mathbf{Y}_t is the label of frame \mathbf{X}_t .

Video Concealed Object Detection (VCOD) [40] is similar to video object detection [41]. This task aims to identify and locate concealed objects within a video by learning a spatial-temporal mapping function $F_{\text{VCOD}} : \{\mathbf{X}_t\}_{t=1}^T \mapsto \{\mathbf{Y}_t\}_{t=1}^T$ that predicts the location \mathbf{Y}_t of an object for each frame \mathbf{X}_t . The location label \mathbf{Y}_t is provided as a bounding box (See Fig. 2 (f)) consisting of four numbers (x, y, w, h) indicating the target’s location. Here, (x, y) represents its top-left coordinate, while w and h denote its width and height, respectively.

Video Concealed Object Segmentation (VCOS) [42] originated from the task of camouflaged object discovery [40]. Its goal is to segment concealed objects within a video. This task usually utilizes spatial-temporal cues to drive the models to learn the mapping $F_{\text{VCOS}} : \{\mathbf{X}_t\}_{t=1}^T \mapsto \{\mathbf{Y}_t\}_{t=1}^T$ between input frames \mathbf{X}_t and corresponding segmentation mask labels \mathbf{Y}_t . Fig. 2 (g) shows an example of its segmentation mask.

In general, compared to image-level CSU, video-level CSU is developing relatively slowly. Because collecting and annotating video data is labor-intensive and time-consuming. However, with the establishment of the first large-scale VCOS benchmark on MoCA-Mask [42], this field has made fundamental progress while still having ample room for exploration.

2.2 Related Topics

Next, we will briefly introduce salient object detection (SOD), which, like COD, requires extracting properties of target objects, but one focuses on saliency while the other on the concealed attribute.

Image-level SOD aims to identify the most attractive objects in an image and extract their pixel-accurate silhouettes [43]. Various network architectures have been explored in deep SOD models, *e.g.*, multi-layer perceptron [44], [45], [46], [47], fully

convolutional [48], [49], [50], [51], [52], capsule-based [53], [54], [55], transformer-based [56], and hybrid [57], [58] networks. Meanwhile, different learning strategies are also studied in SOD models, including data-efficient methods (*e.g.*, weakly-supervised with categorical tags [59], [60], [61], [62], [63] and unsupervised with pseudo masks [64], [65], [66]), multi-task paradigms (*e.g.*, object subitizing [67], [68], fixation prediction [69], [70], semantic segmentation [71], [72], edge detection [73], [74], [75], [76], [77], image captioning [78]), instance-level paradigms [79], [80], [81], [82], *etc*. To learn more about this field comprehensively, readers can refer to popular surveys or representative studies on visual attention [83], saliency prediction [84], co-saliency detection [85], [86], [87], RGB SOD [1], [88], [89], [90], RGB-D (depth) SOD [91], [92], RGB-T (thermal) SOD [93], [94], and light-field SOD [95].

Video-level SOD. The early development of video salient object detection (VSOD) originated from introducing attention mechanisms in video object segmentation (VOS) tasks. At that stage, the task scenes were relatively simple, containing only one object moving in the video. As moving objects tend to attract visual attention, VOS and VSOD were equivalent tasks. For instance, Wang *et al.* [96] used a fully convolutional neural network to address the VSOD task. With the development of VOS techniques, researchers introduced more complex scenes (*e.g.*, with complex backgrounds, object movements, and two objects), but the two tasks remained equivalent. Thus, later works have exploited semantic-level spatial-temporal features [97], [98], [99], [100], recurrent neural networks [101], [102], or offline motion cues such as optical flow [101], [103], [104], [105]. However, with the introduction of more challenging video scenes (containing three or more objects, simultaneous camera, and object movements), VOS and VSOD were no longer equivalent. Yet, researchers continued to approach the two tasks as equivalent, ignoring the issue of visual attention allocation in multi-object movement in video scenes, which seriously hindered the development of the field. To address this issue, in 2019, Fan *et al.* introduced eye trackers to mark the changes in visual attention in multi-object movement scenarios, for the first time posing the scientific problem of *attention shift* [106] in VSOD asks, and constructed the first large-scale VSOD benchmark – DAVSOD¹, as well as the baseline model SSV, which propelled VSOD into a new stage of development.

Remarks. COD and SOD are distinct tasks, but they can mutually benefit via the CamDiff approach [107]. This has been demonstrated through adversarial learning [108], leading to joint research efforts such as the recently proposed dichotomous image segmentation [109]. In §6, we will explore potential directions for future research in these areas.

3 DEEP CSU MODELS

This section systematically reviews deep CSU approaches based on task definitions and data types. We have also created a GitHub base² as a comprehensive collection to provide the latest information in this field.

1. <https://github.com/DengPingFan/DAVSOD>

2. https://github.com/GewelsJI/SINet-V2/blob/main/AWESOME_COD_LIST.md

TABLE 1

Essential characteristics of reviewed image-based methods. This summary outlines the key characteristics, including: **Architecture Design (Arc.):** The framework used, which can be bottom-up & top-down (BTF), multi-stream (MSF), or branched (BF) frameworks. **Multiple Cues (M.C.):** Whether an auxiliary cue is supplied. **Supervision Level (S.L.):** Whether fully-supervised (★) or weakly-supervised (◇) learning is used. **Task Level (T.L.):** The specific tasks addressed by the method, including COS (●), CIS (○), COC (□), and multi-task learning (■). N/A indicates that the source code is not available. For more detailed descriptions of these characteristics, please refer to §3.1 on image-level CSU models.

#	Model	Pub.	Core Component	Arc.	M.C.	S.L.	T.L.	Code
1	ANet [20]	CVIU ₁₉	classification & segmentation streams	BF	✓	★	●	Link
2	SINet [19]	CVPR ₂₀	search and identification modules	BTF	-	★	●	Link
3	MirrorNet [110]	Access ₂₁	fuse input and mirror data streams	MSF	-	★	●	Link
4	DCE [111]	arXiv ₂₁	depth contribution exploration, confidence-aware loss	BF	✓	★	●	Link
5	D2CNet [112]	TIE ₂₁	dual-branch, dual-guidance & cross-refine	BTF	-	★	●	Link
6	C2FNet [113]	IJCAI ₂₁	context-aware cross-level fusion	BTF	-	★	●	Link
7	UR-COD [114]	MMAAsia ₂₁	uncertainty of pseudo-edge labels	MSF	-	★	●	Link
8	TINet [115]	AAAI ₂₁	texture perception & feature interaction guidance	BF	✓	★	●	N/A
9	JSCOD [108]	CVPR ₂₁	uncertainty-aware adversarial learning	MSF	-	★	●	Link
10	LSR [23]	CVPR ₂₁	localize, segment, & rank objects simultaneously	BF	✓	★	■	Link
11	MGL [116]	CVPR ₂₁	mutual graph learning	BF	✓	★	●	Link
12	PFNet [25]	CVPR ₂₁	distraction mining, positioning and focus modules	BTF	-	★	●	Link
13	UGTR [117]	ICCV ₂₁	uncertainty-guided transformer reasoning	BF	✓	★	●	Link
14	BAS [118]	arXiv ₂₂	residual refinement module, hybrid loss	BTF	-	★	●	Link
15	OSFormer [35]	ECCV ₂₂	location-sensing transformer, coarse-to-fine fusion	BF	✓	★	○	Link
16	CFL [36]	TIP ₂₂	camouflage fusion learning	BF	✓	★	○	Link
17	NCHIT [119]	CVIU ₂₂	neighbor connection, hierarchical information transfer	BTF	-	★	●	N/A
18	DTC-Net [120]	TMM ₂₂	local bilinear & spatial coherence organization	BTF	-	★	●	N/A
19	C2FNet-V2 [121]	TCSVT ₂₂	context-aware cross-level fusion	BTF	-	★	●	Link
20	CubeNet [122]	PR ₂₂	encoder-decoder framework with X-connection	BF	✓	★	●	Link
21	ERRNet [123]	PR ₂₂	selective edge aggregation, reversible re-calibration	BF	✓	★	●	Link
22	TPRNet [124]	TVCJ ₂₂	transformer-induced progressive refinement	BTF	-	★	●	Link
23	ANSA-Net [125]	IJCNN ₂₂	attention-based neighbor selective aggregation	BF	✓	★	●	N/A
24	BSANet [126]	AAAI ₂₂	boundary-guided separated attention	BF	✓	★	●	Link
25	FAPNet [127]	TIP ₂₂	boundary guidance, feature aggregation & propagation	BF	✓	★	●	Link
26	FindNet [128]	TIP ₂₂	boundary-and-texture cues (extension of [126])	BF	✓	★	●	N/A
27	PINet [129]	ICME ₂₂	cascaded decamouflage module, label reweighting	BTF	-	★	●	N/A
28	OCENet [130]	WACV ₂₂	online confidence estimation, dynamic uncertainty loss	BF	✓	★	●	Link
29	BGNet [131]	IJCAI ₂₂	edge-guidance feature & context aggregation modules	BF	✓	★	●	Link
30	PreyNet [132]	MM ₂₂	bidirectional bridging interaction, predator learning	BF	✓	★	●	Link
31	DTINet [133]	ICPR ₂₂	dual-task interactive transformer	BF	✓	★	●	Link
32	ZoomNet [134]	CVPR ₂₂	scale integration & hierarchical mixed-scale units	MSF	-	★	●	Link
33	FDNet [135]	CVPR ₂₂	frequency enhancement & high-order relation modules	MSF	-	★	●	N/A
34	SegMaR [136]	CVPR ₂₂	segment, magnify, reiterate in a iterative manner	BTF	-	★	●	Link
35	SINetV2 [22]	TPAMI ₂₂	neighbor connection decoder, group-reversal attention	BTF	-	★	●	Link
36	MGL-V2 [137]	TIP ₂₃	multi-source attention recovery (extension of [116])	BF	✓	★	●	Link
37	FBNet [138]	TMCCA ₂₃	frequency-aware context aggregation & attention	BTF	-	★	●	N/A
38	TANet [139]	TCSVT ₂₃	texture-aware refinement, boundary-consistency loss	BTF	-	★	●	N/A
39	LSR+ [33]	TCSVT ₂₃	triple task learning (extension of [23])	BF	✓	★	■	Link
40	SARNet [140]	TCSVT ₂₃	triple-stage refinement (search-amplify-recognize)	BTF	-	★	●	Link
41	MFFN [141]	WACV ₂₃	co-attention of multi-view, channel fusion unit	MSF	-	★	●	Link
42	CRNet [142]	AAAI ₂₃	feature-guided and consistency losses	MSF	-	◇	●	Link
43	HitNet [143]	AAAI ₂₃	high-resolution iterative feedback	BTF	-	★	●	Link
44	DGNet [28]	MIR ₂₃	gradient-based texture learning, efficient network	BF	✓	★	●	Link
45	FSPNet [144]	CVPR ₂₃	feature shrinkage pyramid with transformer	BTF	-	★	●	Link
46	IOCFormer [39]	CVPR ₂₃	unify density- and regression-based strategies	BF	✓	★	□	Link
47	PFNet+ [26]	SCIS ₂₃	extension of PFNet [25]	BTF	-	★	●	Link
48	DQNet [145]	arXiv ₂₃	cross-model detail querying, relation-based querying	MSF	-	★	●	Link
49	CamoFormer [146]	arXiv ₂₃	masked separable attention	BTF	-	★	●	Link
50	PopNet [147]	arXiv ₂₃	source-free depth, object pop-out prior	MSF	-	★	●	Link

3.1 Image-level CSU Models

We review the existing four image-level CSU tasks: concealed object segmentation (COS), concealed object localization (COL), concealed instance ranking (CIR), and concealed instance segmentation (CIS). Table 1 summarizes the key features of these reviewed approaches.

3.1.1 Concealed Object Segmentation

This section discusses previous solutions for camouflage object segmentation (COS) from two perspectives: network architecture and learning paradigm.

Network Architecture. Generally, fully convolutional networks (FCNs [148]) are the standard solution for image segmentation as they can receive input of a flexible size and undergo a single feed-forward propagation. As expected, FCN-shaped frameworks dominate the primary solutions for COS, which fall into three categories: *a) Multi-stream framework*, shown

in Fig. 3 (a), contains multiple input streams to learn multi-source representations explicitly. MirrorNet [110] was the first attempt to add an extra data stream as a bio-inspired attack, which can break the camouflaged state. Several recent works have adopted a multi-stream approach to improve their results, such as supplying pseudo-depth generation [147], pseudo-edge uncertainty [114], adversarial learning paradigm [108], frequency enhancement stream [135]), multi-scale [134] or multi-view [141] inputs, and multiple backbones [145]. *b) Bottom-up and top-down framework*, as shown in Fig. 3 (b), uses deeper features to enhance shallower ones gradually in a single feed-forward pass. For example, C2FNet [113] adopts this design to improve concealed features from coarse-to-fine levels. In addition, SegMaR [136] employs an iterative refinement network with a sub-network based on this strategy. Furthermore, other studies [19], [22], [25], [26], [112], [118], [119], [120], [121], [124], [125], [129], [138], [139], [140], [143], [144], [146] utilized a deeply-supervised

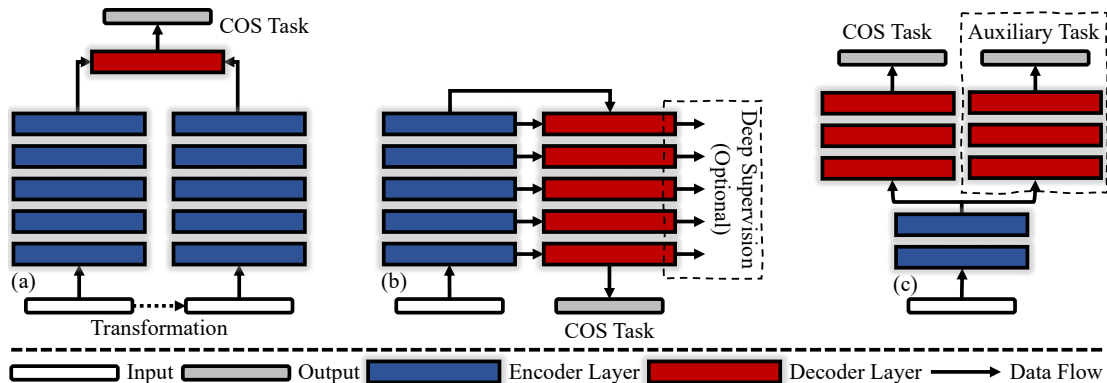


Fig. 3. **Network architectures for COS at a glance.** We present four types of frameworks from left to right: (a) multi-stream framework, (b) bottom-up/top-down framework and its variant with deep supervision (optional), and (c) branched framework. See §3.1.1 for more details.

strategy [149], [150] on various intermediate feature hierarchies using this framework. This practical, also utilized by the feature pyramid network [151], combines more comprehensive multi-context features through dense top-down and bottom-up propagation and introduces additional supervision signals before final prediction to provide more dependable guidance for deeper layers. **c) Branched framework**, shown in Fig. 3 (c), is a single-input-multiple-output architecture, consisting of both segmentation and auxiliary task branches. It should be noted that the segmentation part of this branched framework may have some overlap with previous frameworks, such as single-stream [20] and bottom-up & top-down [23], [28], [33], [108], [111], [115], [116], [117], [122], [123], [125], [126], [127], [128], [130], [131], [132], [133], [137] frameworks. For instance, ERRNet [123] and FAPNet [127] are typical examples of jointly learning concealed objects and their boundaries. Since these branched frameworks are closely related to the multi-task learning paradigm, we will provide details.

Learning Paradigm. Next, we discuss three common types of learning paradigms for COS tasks: single-task, multi-task, and data-efficient learning. **1) Single-task learning** is the most commonly used paradigm in COS, which involves only a segmentation task for concealed targets. Based on this paradigm, most current works [19], [22], [121] focus on developing attention modules to identify target regions. **2) Multi-task learning** introduces an auxiliary task to coordinate or complement the segmentation task, leading to robust COS learning. These multi-task frameworks can be implemented by conducting confidence estimation [108], [117], [130], [132], localization/ranking [23], [33], category prediction [20] tasks and learning depth [111], [147], boundary [116], [122], [123], [126], [127], [131], and texture [28], [115] cues of camouflaged object. **3) Data-efficient learning** is capable of comprehending complex data distributions without requiring large amounts of annotated data, unlike the single- and multi-task frameworks mentioned before, which operate under fully-supervised settings. This approach helps alleviate over-fitting problems on limited knowledge annotated data. CRNet [142] is the only weakly-supervised framework utilizing scribble labels as supervision.

3.1.2 Concealed Instance Ranking

There has been limited research conducted on this topic. Lv *et al.* [23] observed for the first time existing COS approaches could not quantify the difficulty level of camouflage. Regarding

this issue, they used an eye tracker to create a new dataset, called CAM-LDR [33], that contains instance segmentation masks, fixation labels, and ranking labels. They also proposed two unified frameworks, LSR [23] and its extension LSR+ [33], to simultaneously learn triple tasks, *i.e.*, localizing, segmenting, and ranking camouflaged objects. The insight behind it is that discriminative localization regions could guide the segmentation of the full scope of camouflaged objects, and then, the detectability of different camouflaged objects could be inferred by the ranking task.

3.1.3 Concealed Instance Segmentation

This task advances the COS task from the regional to the instance level, a relatively new field compared with the COS. Then, Le *et al.* [36] build a new CIS benchmark, CAMO++, via extending on previous CAMO [20] dataset. They also proposed a camouflage fusion learning strategy to fine-tune existing instance segmentation models (*e.g.*, Mask R-CNN [34]) by learning image contexts. Recently, on the basis of instance benchmarks as in COD10K [19] and NC4K [23], the first one-stage transformer framework, OSFormer [35], was proposed for this field by introducing two core designs: location-sensing transformer and coarse-to-fine fusion.

3.1.4 Concealed Object Counting

Sun *et al.* [39] recently introduced a new challenge for the community called indiscernible object counting (IOC), which involves counting objects that are difficult to distinguish from their surroundings. They created IOCfish5K, a large-scale dataset containing high-resolution images of underwater scenes with many indiscernible objects (focus on fish) and dense annotations to address the lack of appropriate datasets for this challenge. They also proposed a baseline model, IOCFormer, by integrating density-based and regression-based methods in a unified framework.

Based on the above summaries, the COS task is experiencing a rapid development period, resulting in numerous contemporary publications each year. However, very few proposed solutions are still proposed for the COL, CIR, and CIS tasks. This suggests that these fields remain under-explored and offer significant room for further research. Notably, many previous studies are available as references (such as saliency prediction [84], salient object subitizing [68], and salient instance segmentation [82]), providing a solid foundation for understanding these tasks from a camouflaged perspective.

TABLE 2

Essential characteristics of reviewed video-level methods. Optical flow (O.F.): whether pre-generating optical flow map. **Supervision level (S.L.):** fully-supervision with real data (★) or synthetic data (♣), and self-supervision (♡). **Task level (T.L.):** video camouflaged object detection (△) and segmentation (▲). For further details, refer to §3.2.

#	Model	Pub.	Core Components	O.F.	S.L.	T.L.	Project
1	FMC [152]	CVPR ₁₉	pixel trajectory recurrent neural network and clustering	✓	★	▲	N/A
2	VRS [40]	ACCV ₂₀	video registration and motion segmentation network	✓	★	△	Link
3	SIMO [153]	BMVC ₂₁	dual-head architecture, synthetic dataset	✓	♣	△	Link
4	MG [154]	ICCV ₂₁	self-supervised motion grouping	✓	♡	△	Link
5	RCF [155]	arXiv ₂₂	rotation-compensated flow, camera motion estimation	✓	★	△	N/A
6	OCLR [156]	NeurIPS ₂₂	object-centric layered representation, synthetic dataset	✓	♣	△	N/A
7	OFS [157]	TPAMI ₂₂	expectation-maximization method, motion augmentation	✓	♡	△	Link
8	QSDI [158]	CVPR ₂₂	quantifying the static and dynamic biases	✓	★	△	Link
9	SLTNet [42]	CVPR ₂₂	implicit motion handling, short- and long-term modules	-	★	▲	Link

3.2 Video-level CSU Models

There are two branches for the video-level CSU task, including detecting and segmenting camouflaged objects from videos. Refer Table 2 for details.

3.2.1 Video Concealed Object Detection

Most works [154], [156] formulated this topic as the degradation problem of the segmentation task since the scarcity of pixel-wise annotations. They, as usual, trained on segmentation datasets (e.g., DAVIS [159], FBMS [160]) but evaluated the generalizability performance on video camouflaged object detection dataset, MoCA [40]. These methods consistently opt to extract offline optical flow as motion guidance for the segmentation task, but diversifying over the learning strategies, such as fully-supervised learning with real [40], [155], [158] or synthetic [153], [156] data and self-supervised learning [154], [157].

3.2.2 Video Concealed Object Segmentation

Xie *et al.* [152] proposed the first work on camouflaged object discovery in videos. They used a pixel-trajectory recurrent neural network to cluster foreground motion for segmentation. However, this work is limited to a small-scale dataset, CAD [161]. Recently, based upon localization-level dataset MoCA [40] with bounding box labels, Cheng *et al.* [42] extended this field by creating a large-scale VCOS benchmark MoCA-Mask with pixel-level masks. They also introduced a two-stage baseline SLTNet to implicitly utilize motion information.

From what we have reviewed above, the current approaches for VCOS tasks are still in a nascent state of development. Several concurrent works in well-established video segmentation fields (e.g., self-supervised correspondence learning [162], [163], [164], [165], [166], unified framework for different motion-based tasks [167], [168], [169]) points the way to further explore. Besides, considering high-level semantic understanding has a research gap that merits being supplied, such as semantic segmentation and instance segmentation in the camouflaged scenes.

4 CSU DATASETS

In recent years, various datasets have been collected for both image- and video-level CSU tasks. In Table 3, we summarize the features of the representative datasets.

4.1 Image-level Datasets

- **CAMO-COCO** [20] is tailor-made for COS tasks with 2,500 image samples across eight categories, divided into two sub-datasets, *i.e.*, CAMO with camouflaged objects and MS-COCO

with non-camouflaged objects. Both CAMO and MS-COCO contain 1,250 images with a split of 1,000 for training and 250 for testing.

NC4K [23] is currently the largest testing set for evaluating COS models. NC4K consists of 4,121 camouflaged images sourced from the Internet and can be divided into two primary categories: natural scenes and artificial scenes. In addition to the images, this dataset also provides localization labels that include both object-level segmentation and instance-level masks, making it a valuable resource for researchers working in this field. In a recent study by Lv *et al.* [23], an eye tracker was utilized to collect fixation information for each image. As a result, a CAM-FR dataset of 2,280 images was created, with 2,000 images used for training and 280 for testing. The dataset was annotated with three types of labels: localization, ranking, and instance labels.

CAMO++ [36] is a newly released dataset that contains 5,500 samples, all of which have undergone hierarchical pixel-wise annotation. The dataset is divided into two parts: camouflaged samples (1,700 images for training and 1,000 for testing) and non-camouflaged samples (1,800 images for training and 1,000 for testing).

COD10K [19], [22] is currently the largest-scale dataset, featuring a wide range of camouflaged scenes. The dataset contains 10,000 images from multiple open-access photography websites, covering ten super-classes and 78 sub-classes. Out of these images, 5,066 are camouflaged, 1,934 are non-camouflaged pictures and 3,000 are background images. The camouflaged subset of COD10K is annotated using different labels such as category labels, bounding boxes, object-level masks, and instance-level masks, providing a diverse set of annotations.

CAM-LDR [33] comprises of 4,040 training and 2,026 testing samples. These samples were selected from commonly-used hybrid training datasets (*i.e.*, CAMO with 1,000 training samples and COD10K with 3,040 training samples), along with the testing dataset (*i.e.*, COD10K with 2,026 testing samples). CAM-LDR is an extension of NC4K [23] that includes four types of annotations: localization labels, ranking labels, object-level segmentation masks, and instance-level segmentation masks. The ranking labels are categorized into six difficulty levels – background, easy, medium1, medium2, medium3, and hard.

S-COD [142] is the first dataset designed specifically for the COS task under the weakly-supervised setting. The dataset includes 4,040 training samples, with 3,040 samples selected from COD10K and 1,000 from CAMO. These samples were re-labeled using scribble annotations that provide a rough outline of the

TABLE 3

Essential characteristics for CSU datasets. **Train/Test:** number of samples for training/testing (e.g., images for image dataset or frames for video dataset) **Task:** data type of dataset. **N.Cam.:** whether collecting non-camouflaged samples. **Cls.:** whether providing classification labels. **B.Box:** whether providing bounding box labels for the detection task. **Obj./Ins.:** whether providing object- or instance-level segmentation masks for segmentation tasks. **Rank:** whether providing ranking labels for instances. **Scr.:** whether providing weak labels in scribbled form. **Cou.:** whether providing dense object counting labels. See §4.1 and §4.2 for more descriptions.

#	Dataset	Year	Pub.	Train	Test	Task	N.Cam.	Cls.	B.Box	Obj.	Ins.	Fix.	Rank	Scr.	Cou.	Website
1	CAD [161]	2016	ECCV	0	836	Video	-	✓	-	✓	-	-	-	-	-	Link
2	CAMO-COCO [20]	2019	CVIU	2000	500	Image	✓	-	-	✓	-	-	-	-	-	Link
3	MoCA [40]	2020	ACCV	0	37,250	Video	-	✓	✓	-	-	-	-	-	-	Link
4	NC4K [23]	2021	CVPR	0	4,121	Image	-	-	✓	✓	✓	-	-	-	-	Link
5	MoCA-Mask [42]	2022	CVPR	19,313	3,626	Video	-	✓	-	✓	-	-	-	-	-	Link
6	CAMO++ [36]	2022	TIP	3,500	2,000	Image	✓	-	✓	✓	-	-	-	-	-	Link
7	COD10K [19], [22]	2022	TPAMI	6,000	4,000	Image	✓	✓	✓	✓	✓	-	-	-	-	Link
8	CAM-LDR [33]	2023	TCSVT	4,040	2,026	Image	-	-	-	✓	✓	✓	✓	-	-	Link
9	S-COD [142]	2023	AAAI	4,040	0	Image	-	-	-	-	-	-	-	✓	-	Link
10	Camfish5K [39]	2023	CVPR	3,637	2,000	Image	-	✓	-	-	-	-	-	-	✓	Link

primary structure based on first impressions, without pixel-wise ground-truth information.

Camfish5K [39] is a distinct dataset that focuses on counting instances of fish in camouflaged scenes. This COC dataset comprises 5,637 high-resolution images collected from YouTube, with 659,024 center points annotated. The dataset is divided into three subsets, with 3,137 images allocated for training, 500 for validation, and 2,000 for testing.

Remarks. In summary, three datasets (CAMO, COD10K, and NC4K) are commonly used as benchmarks to evaluate camouflage object segmentation (COS) approaches, with the experimental protocols typically described in §5.2. For the concealed instance segmentation (CIS) task, two datasets (COD10K and NC4K) containing instance-level segmentation masks can be utilized. The CAM-LDR dataset, which provides fixation information and three types of annotations collected from a physical eye tracker device, is suitable for various brain-inspired explorations in computer vision. Additionally, there are two new datasets from CSU: S-COD, designed for weakly-supervised COS, and Camfish5K, focused on counting objects within camouflaged scenes.

4.2 Video-level Datasets

- **CAD** [161] is a small dataset comprising nine short video clips and 836 frames. The annotation strategy used in this dataset is sparse, with camouflaged objects being annotated every five frames. As a result, there are 191 segmentation masks available in the dataset.

MoCA [40] is a comprehensive video database from YouTube that aims to detect moving camouflaged animals. It consists of 141 video clips featuring 67 categories and comprises 37,250 high-resolution frames with corresponding bounding box labels for 7,617 instances.

MoCA-Mask [42], an extension of MoCA dataset [40], provides human-annotated segmentation masks every five frames based on MoCA dataset [40]. MoCA-Mask is divided into two parts: a training set consisting of 71 short clips (19,313 frames with 3,946 segmentation masks) and an evaluation set containing 16 short clips (3,626 frames with 745 segmentation masks). To label those unlabeled frames, pseudo-segmentation labels were synthesized using a bidirectional optical flow-based strategy [170].

Remarks. The MoCA dataset is currently the largest collection of videos with concealed objects, while it only offers detection labels.

As a result, researchers in the community [154], [156] typically assess the performance of well-trained segmentation models by converting segmentation masks into detection bounding boxes. Recently, there has been a shift towards video segmentation in concealed scenes with the introduction of MoCA-Mask. Despite these advancements, the quantity and quality of data annotations remain insufficient for constructing a reliable video model that can effectively handle complex concealed scenarios.

5 CSU BENCHMARKS

In this investigation, our benchmarking is built on COS tasks since this topic is relatively well-established and offers a variety of competing approaches. The following sections will detail the evaluation metrics (§5.1), benchmarking protocols (§5.2), quantitative analyses (§5.3, §5.4, §5.5), and qualitative comparisons (§5.6).

5.1 Evaluation Metrics

Suggested by [22], there are five commonly used metrics³ available for COS evaluation. We compare a prediction mask \mathbf{P} with its corresponding ground-truth mask \mathbf{G} at the same image resolution.

MAE (mean absolute error, M) is a conventional pixel-wise measure, which is defined as:

$$M = \frac{1}{W \times H} \sum_x \sum_y^W |P(x,y) - G(x,y)|, \quad (1)$$

where W and H are the width and height of \mathbf{G} , and (x,y) are pixel coordinates in \mathbf{G} .

F-measure could be defined as:

$$F_\beta = \frac{(1 + \beta^2) \text{Precision} \times \text{Recall}}{\beta^2 \text{Precision} + \text{Recall}}, \quad (2)$$

where $\beta^2 = 0.3$ is used to emphasize precision value over recall value, as recommended in [90]. Other two metrics are derived:

$$\text{Precision} = \frac{|\mathbf{P}(T) \cap \mathbf{G}|}{|\mathbf{P}(T)|}, \quad \text{Recall} = \frac{|\mathbf{P}(T) \cap \mathbf{G}|}{|\mathbf{G}|}, \quad (3)$$

where $\mathbf{P}(T)$ is a binary mask obtained by thresholding the non-binary predicted map \mathbf{P} with a threshold value $T \in [0, 255]$. The symbol $|\cdot|$ calculates the total area of the mask inside the map. Therefore, it is possible to convert a non-binary prediction mask into a series of binary masks with threshold values ranging from 0

3. https://github.com/DengPingFan/CSU/tree/main/cos_eval_toolbox

TABLE 4

Quantitative comparison on CAMO [20] testing set. We classify the competing approaches based on two aspects: those using convolution-based backbones such as ResNet [173], Res2Net [174], EffNet [175], and ConvNext [176]; and those using transformer-based backbones such as MiT [177], PVTv2 [178], and Swin [179]. We test two efficiency metrics, model parameters (Para) and multiply-accumulate operations (MACs), in accordance with the preset input resolution in the original paper. Besides, nine evaluation metrics are reported, and the best three scores are highlighted in **red**, **green**, and **blue**, respectively, with \uparrow/\downarrow indicating that higher/lower scores are better. If the results are unavailable since the code has not been public, we use a hyphen (-) to denote it. We will follow these notations in subsequent tables unless otherwise specified.

Model	Pub/Year	Backbone	Input	Para.	MACs	$S_\alpha \uparrow$	$F_\beta^w \uparrow$	$M \downarrow$	$E_\phi^{ad} \uparrow$	$E_\phi^{mn} \uparrow$	$E_\phi^{mx} \uparrow$	$F_\beta^{ad} \uparrow$	$F_\beta^{mn} \uparrow$	$F_\beta^{mx} \uparrow$
• Convolution-based Backbone														
SINet [19]	CVPR ₂₀	ResNet-50	352 ²	48.95M	19.42G	0.745	0.644	0.092	0.825	0.804	0.829	0.712	0.702	0.708
D2CNet [112]	TIE ₂₁	Res2Net-50	320 ²	-	-	0.774	0.683	0.087	0.844	0.818	0.838	0.747	0.735	0.743
C2FNet [113]	IJCAI ₂₁	Res2Net-50	352 ²	28.41M	13.12G	0.796	0.719	0.080	0.865	0.854	0.864	0.764	0.762	0.771
TINet [115]	AAAI ₂₁	ResNet-50	352 ²	28.56M	8.58G	0.781	0.678	0.087	0.847	0.836	0.848	0.729	0.728	0.745
JSCOD [108]	CVPR ₂₁	ResNet-50	352 ²	121.63M	25.20G	0.800	0.728	0.073	0.872	0.859	0.873	0.779	0.772	0.779
LSR [23]	CVPR ₂₁	ResNet-50	352 ²	57.90M	25.21G	0.787	0.696	0.080	0.859	0.838	0.854	0.756	0.744	0.753
R-MGL [116]	CVPR ₂₁	ResNet-50	473 ²	67.64M	249.89G	0.775	0.673	0.088	0.848	0.812	0.842	0.738	0.726	0.740
S-MGL [116]	CVPR ₂₁	ResNet-50	473 ²	63.60M	236.60G	0.772	0.664	0.089	0.850	0.807	0.842	0.733	0.721	0.739
PFNet [25]	CVPR ₂₁	ResNet-50	416 ²	46.50M	26.54G	0.782	0.695	0.085	0.855	0.841	0.855	0.751	0.746	0.758
UGTR [117]	ICCV ₂₁	ResNet-50	473 ²	48.87M	127.12G	0.785	0.686	0.086	0.861	0.823	0.854	0.749	0.738	0.754
BAS [118]	arXiv ₂₁	ResNet-34	288 ²	87.06M	161.19G	0.749	0.646	0.096	0.808	0.796	0.808	0.696	0.692	0.703
NCHIT [119]	CVIU ₂₂	ResNet-50	288 ²	-	-	0.784	0.652	0.088	0.841	0.805	0.840	0.723	0.707	0.739
C2FNet-V2 [121]	TCSVT ₂₂	Res2Net-50	352 ²	44.94M	18.10G	0.799	0.730	0.077	0.869	0.859	0.869	0.777	0.770	0.779
CubeNet [122]	PR ₂₂	ResNet-50	352 ²	-	-	0.788	0.682	0.085	0.852	0.838	0.860	0.734	0.732	0.750
ERRNet [123]	PR ₂₂	ResNet-50	352 ²	69.76M	20.05G	0.779	0.679	0.085	0.855	0.842	0.858	0.731	0.729	0.742
TPRNet [124]	TVCJ ₂₂	Res2Net-50	352 ²	32.95M	12.98G	0.807	0.725	0.074	0.880	0.861	0.883	0.777	0.772	0.785
FAPNet [127]	TIP ₂₂	Res2Net-50	352 ²	29.52M	29.69G	0.815	0.734	0.076	0.877	0.865	0.880	0.776	0.776	0.792
BSANet [126]	AAAI ₂₂	Res2Net-50	384 ²	32.58M	29.70G	0.794	0.717	0.079	0.866	0.851	0.867	0.768	0.763	0.770
OCENet [130]	WACV ₂₂	ResNet-50	480 ²	60.31M	59.70G	0.802	0.723	0.080	0.866	0.852	0.865	0.776	0.766	0.777
BGNet [131]	IJCAI ₂₂	Res2Net-50	416 ²	79.85M	58.45G	0.812	0.749	0.073	0.876	0.870	0.882	0.786	0.789	0.799
PreyNet [132]	MM ₂₂	ResNet-50	448 ²	38.53M	58.10G	0.790	0.708	0.077	0.856	0.842	0.857	0.763	0.757	0.765
ZoomNet [134]	CVPR ₂₂	ResNet-50	384 ²	32.38M	95.50G	0.820	0.752	0.066	0.883	0.877	0.892	0.792	0.794	0.805
FDNet [135]	CVPR ₂₂	Res2Net-50	416 ²	-	-	0.841	0.775	0.063	0.901	0.895	0.908	0.803	0.807	0.826
SegMaR [136]	CVPR ₂₂	ResNet-50	352 ²	56.21M	33.63G	0.815	0.753	0.071	0.881	0.874	0.884	0.795	0.795	0.803
SINetV2 [22]	TPAMI ₂₂	Res2Net-50	352 ²	26.98M	12.28G	0.820	0.743	0.070	0.884	0.882	0.895	0.779	0.782	0.801
CamoFormer-C [146]	arXiv ₂₃	ConvNeXt-B	384 ²	96.69M	50.77G	0.859	0.812	0.050	0.919	0.913	0.920	0.842	0.842	0.855
CamoFormer-R [146]	arXiv ₂₃	ResNet-50	384 ²	54.25M	78.85G	0.816	0.712	0.076	0.863	0.874	0.916	0.735	0.745	0.813
PopNet [147]	arXiv ₂₃	Res2Net-50	512 ²	188.05M	154.88G	0.808	0.744	0.077	0.871	0.859	0.874	0.790	0.784	0.792
CRNet [142]	AAAI ₂₃	ResNet-50	320 ²	32.65M	11.83G	0.735	0.641	0.092	0.829	0.815	0.830	0.709	0.701	0.707
PFNet+ [26]	SCIS ₂₃	ResNet-50	480 ²	-	-	0.791	0.713	0.080	0.862	0.850	0.865	0.764	0.761	0.770
DGNet-S [28]	MIR ₂₃	EffNet-B1	352 ²	7.02M	2.77G	0.826	0.754	0.063	0.896	0.893	0.907	0.786	0.792	0.810
DGNet [28]	MIR ₂₃	EffNet-B4	352 ²	19.22M	1.20G	0.839	0.769	0.057	0.906	0.901	0.915	0.804	0.806	0.822
• Transformer-based Backbone														
DTINet [133]	ICPR ₂₂	MiT-B5	256 ²	266.33M	144.68G	0.856	0.796	0.050	0.918	0.916	0.927	0.821	0.823	0.843
CamoFormer-S [146]	arXiv ₂₃	Swin-B	384 ²	97.27M	64.13G	0.876	0.832	0.043	0.935	0.930	0.938	0.856	0.856	0.871
CamoFormer-P [146]	arXiv ₂₃	PVTv2-B4	384 ²	71.40M	39.74G	0.872	0.831	0.046	0.931	0.929	0.938	0.853	0.854	0.868
HitNet [143]	AAAI ₂₃	PVTv2-B2	704 ²	25.73M	55.95G	0.849	0.809	0.055	0.910	0.906	0.910	0.833	0.831	0.838

to 255. By iterating over all thresholds, three metrics are obtained with maximum value (F_β^{mx}), mean value (F_β^{mn}), and adaptive value (F_β^{ad}) of F-measure.

Enhanced-alignment measure (E_ϕ) [171], [172] is a recently proposed binary foreground evaluation metric, which considers the both local and global similarity between two binary maps. Its formulation is defined as:

$$E_\phi = \frac{1}{W \times H} \sum_x \sum_y \phi [\mathbf{P}(x, y), \mathbf{G}(x, y)], \quad (4)$$

where ϕ is the enhanced-alignment matrix. Similar to F_β , this metric also includes three values computed over all the thresholds, *i.e.*, maximum (E_ϕ^{mx}), mean (E_ϕ^{mn}), and adaptive (E_ϕ^{ad}) values.

Structure measure (S_α) [180], [181] is used to measure the structural similarity between a non-binary prediction map and a ground-truth mask:

$$S_\alpha = (1 - \alpha)S_o(\mathbf{P}, \mathbf{G}) + \alpha S_r(\mathbf{P}, \mathbf{G}), \quad (5)$$

where α balances the object-aware similarity S_o and region-aware similarity S_r . As in the original paper, we use the default setting for $\alpha = 0.5$.

5.2 Experimental Protocols

Suggested by Fan *et al.* [22], all competing approaches in the benchmarking were trained on a hybrid dataset comprising the training portions of COD10K [19] and CAMO [20] datasets, totaling 4,040 samples. The models were then evaluated on three popular used benchmarks: COD10K's testing portion with 2,026 samples [19], CAMO with 250 samples [20], and NC4K with 4,121 samples [23].

5.3 Quantitative Analysis on CAMO

As reported in Table 4, we evaluated 36 deep-based approaches on the CAMO testing dataset [20] using various metrics. These models were classified into two groups based on the backbones they used: 32 convolutional-based and four transformer-based. As for those models using convolutional-based backbones, several interesting findings are observed:

- CamoFormer-C [146] achieved the best performance on CAMO with the ConvNeXt [176] based backbone, even surpassing some metrics produced by transformer-based methods, such as S_α value: 0.859 (CamoFormer-C) *vs.* 0.856 (DTINet [133]) *vs.* 0.849 (HitNet [143]). However, CamoFormer-R [146] with ResNet-50 backbone was unable to outperform competitors with the same

TABLE 5
Quantitative comparison on NC4K [23] testing dataset.

Model	Pub/Year	Backbone	$S_\alpha \uparrow$	$F_\beta^w \uparrow$	$M \downarrow$	$E_\phi^{ad} \uparrow$	$E_\phi^{mn} \uparrow$	$E_\phi^{mx} \uparrow$	$F_\beta^{ad} \uparrow$	$F_\beta^{mn} \uparrow$	$F_\beta^{mx} \uparrow$
• Convolution-based Backbone											
SINet [19]	CVPR ₂₀	ResNet-50	0.808	0.723	0.058	0.883	0.871	0.883	0.768	0.769	0.775
C2FNet [113]	IJCAI ₂₁	Res2Net-50	0.838	0.762	0.049	0.901	0.897	0.904	0.788	0.795	0.810
TINet [115]	AAAI ₂₁	ResNet-50	0.829	0.734	0.055	0.882	0.879	0.890	0.766	0.773	0.793
JSCOD [108]	CVPR ₂₀	ResNet-50	0.842	0.771	0.047	0.906	0.898	0.907	0.803	0.806	0.816
LSR [23]	CVPR ₂₁	ResNet-50	0.840	0.766	0.048	0.904	0.895	0.907	0.802	0.804	0.815
R-MGL [116]	CVPR ₂₁	ResNet-50	0.833	0.740	0.052	0.890	0.867	0.893	0.778	0.782	0.800
S-MGL [116]	CVPR ₂₁	ResNet-50	0.829	0.731	0.055	0.885	0.863	0.893	0.771	0.777	0.797
PFNet [25]	CVPR ₂₁	ResNet-50	0.829	0.745	0.053	0.894	0.887	0.898	0.779	0.784	0.799
UGTR [117]	ICCV ₂₁	ResNet-50	0.839	0.747	0.052	0.889	0.874	0.899	0.779	0.787	0.807
BAS [118]	arXiv ₂₁	ResNet-34	0.817	0.732	0.058	0.868	0.859	0.872	0.767	0.772	0.782
NCHIT [119]	CVIU ₂₂	ResNet-50	0.830	0.710	0.058	0.872	0.851	0.894	0.751	0.758	0.792
C2FNet-V2 [121]	TCSVT ₂₂	Res2Net-50	0.840	0.770	0.048	0.900	0.896	0.904	0.799	0.802	0.814
ERRNet [123]	PR ₂₂	ResNet-50	0.827	0.737	0.054	0.892	0.887	0.901	0.769	0.778	0.794
TPRNet [124]	TVCJ ₂₂	Res2Net-50	0.846	0.768	0.048	0.901	0.898	0.911	0.798	0.805	0.820
FAPNet [127]	TIP ₂₂	Res2Net-50	0.851	0.775	0.047	0.903	0.899	0.910	0.804	0.810	0.826
BSANet [126]	AAAI ₂₂	Res2Net-50	0.841	0.771	0.048	0.906	0.897	0.907	0.805	0.808	0.817
OCENet [130]	WACV ₂₂	ResNet-50	0.853	0.785	0.045	0.908	0.902	0.913	0.812	0.818	0.831
BGNet [131]	IJCAI ₂₂	Res2Net-50	0.851	0.788	0.044	0.911	0.907	0.916	0.813	0.820	0.833
PreyNet [132]	MM ₂₂	ResNet-50	0.834	0.763	0.050	0.899	0.887	0.899	0.805	0.803	0.811
ZoomNet [134]	CVPR ₂₂	ResNet-50	0.853	0.784	0.043	0.907	0.896	0.912	0.814	0.818	0.828
FDNet [135]	CVPR ₂₂	Res2Net-50	0.834	0.750	0.052	0.895	0.893	0.905	0.774	0.784	0.804
SegMaR [136]	CVPR ₂₂	ResNet-50	0.841	0.781	0.046	0.905	0.896	0.907	0.821	0.821	0.826
SINetV2 [22]	TPAMI ₂₂	Res2Net-50	0.847	0.770	0.048	0.901	0.903	0.914	0.792	0.805	0.823
CamoFormer-C [146]	arXiv ₂₃	ConvNeXt-B	0.883	0.834	0.032	0.937	0.933	0.940	0.851	0.857	0.870
CamoFormer-R [146]	arXiv ₂₃	ResNet-50	0.855	0.788	0.042	0.913	0.900	0.914	0.820	0.821	0.830
PopNet [147]	arXiv ₂₃	Res2Net-50	0.861	0.802	0.042	0.915	0.909	0.919	0.830	0.833	0.843
DGNet-S [28]	MIR ₂₃	EfficientNet-B1	0.845	0.764	0.047	0.902	0.902	0.913	0.789	0.799	0.819
DGNet [28]	MIR ₂₃	EfficientNet-B4	0.857	0.784	0.042	0.910	0.911	0.922	0.803	0.814	0.833
• Transformer-based Backbone											
DTINet [133]	ICPR ₂₂	MiT-B5	0.863	0.792	0.041	0.914	0.917	0.926	0.809	0.818	0.836
CamoFormer-S [146]	arXiv ₂₃	Swin-B	0.888	0.840	0.031	0.941	0.937	0.946	0.857	0.863	0.877
CamoFormer-P [146]	arXiv ₂₃	PVTv2-B4	0.892	0.847	0.030	0.941	0.939	0.946	0.863	0.868	0.880
HitNet [143]	AAAI ₂₃	PVTv2-B2	0.875	0.834	0.037	0.928	0.926	0.929	0.854	0.853	0.863

backbone, such as using multi-scale zooming (ZoomNet [134]) and iterative refinement (SegMaR [136]) strategies.

- As for those Res2Net-based models, FDNet [135] achieves the top performance on CAMO with high-resolution input of 416^2 . Besides, SINetV2 [22] and FAPNet [127] achieve satisfactory performance using the same backbone but with a small input resolution of 352^2 .

- DGNet [28], is an efficient model that stands out with its top#3 performance compared to heavier models like JSCOD [108] (121.63M) and PopNet [147] (181.05M), despite having only 19.22M parameters and 1.20G computation costs. Its performance-efficiency balance makes it a promising architecture for further exploration of its potential capabilities.

- Interestingly, CRNet [142] – a weakly-supervised model – competes favorably with early fully-supervised model SINet [19]. It suggests that there is room for developing models to bridge the gap toward better data-efficient learning, such as self-/semi-supervised learning.

Furthermore, transformer-based methods significantly improve performance due to their superior long-range modeling capabilities. We here test four transformer-based models on the CAMO testing dataset, yielding three noteworthy findings:

- CamoFormer-S [146], utilizes a Swin transformer design to enhance the hierarchical modeling ability on concealed content, resulting in superior performance across the entire CAMO benchmark. We also observed that the PVT-based variant CamoFormer-P [146] achieves comparable results but with fewer parameters, *i.e.*, 71.40M (CamoFormer-P) vs. 97.27M (CamoFormer-R).

- DTINet [133] is a dual-branch network that utilizes the MiT-B5 semantic segmentation model from SegFormer [177] as backbone. Despite having 266.33M parameters, it has not delivered impres-

sive performance due to the challenges of balancing such two heavy branches. Nevertheless, this attempt defies our preconceptions and inspires us to investigate the transferability of semantic segmentation models in concealed scenarios.

- We also investigate the impact of input resolution on the performance of different models. HitNet [143] uses a high-resolution image of 704^2 , which can improve the detection of small targets, but at the expense of increased computation costs. Similarly, convolutional-based approaches like ZoomNet [134] achieved impressive results by taking multiple inputs with different resolutions (the largest being 576^2) to enhance segmentation performance. However, not all models benefit from this approach. For instance, PopNet [147] with a resolution of 480^2 fails to outperform SINetV2 [22] with 352^2 in all metrics. This observation raises two critical questions: should high-resolution be used in concealed scenarios, and how can we develop an effective strategy for detecting concealed objects of varying sizes? We will propose potential solutions to these questions and present an interesting analysis of the COD10K in §5.5.

5.4 Quantitative Analysis on NC4K

Compared to the CAMO dataset, the NC4K [23] dataset has a larger data scale and sample diversity, indicating subtle changes may have occurred. Table 5 presents quantitative results on the current largest COS testing dataset with 4,121 samples. The benchmark includes 28 convolutional-based and four transformer-based approaches. Our observations are:

- CamoFormer-C [146] still outperforms all methods on NC4K. In contrast to the awkward situation observed on CAMO as described in §5.3, the ResNet-50 based CamoFormer-R [146] now performs

TABLE 6
Quantitative comparison on COD10K [19] testing set.

Model	Pub/Year	Backbone	$S_\alpha \uparrow$	$F_\beta^w \uparrow$	$M \downarrow$	$E_\phi^{ad} \uparrow$	$E_\phi^{mn} \uparrow$	$E_\phi^{mx} \uparrow$	$F_\beta^{ad} \uparrow$	$F_\beta^{mn} \uparrow$	$F_\beta^{mx} \uparrow$
• Convolution-based Backbone											
SINet [19]	CVPR ₂₀	ResNet-50	0.776	0.631	0.043	0.867	0.864	0.874	0.667	0.679	0.691
D2CNet [112]	TIE ₂₁	ResNet-50	0.807	0.680	0.037	0.879	0.876	0.887	0.702	0.720	0.736
C2FNet [113]	IJCAI ₂₁	Res2Net-50	0.813	0.686	0.036	0.886	0.890	0.900	0.703	0.723	0.743
TINet [115]	AAAI ₂₁	ResNet-50	0.793	0.635	0.042	0.848	0.861	0.878	0.652	0.679	0.712
JSCOD [108]	CVPR ₂₀	ResNet-50	0.809	0.684	0.035	0.882	0.884	0.891	0.705	0.721	0.738
LSR [23]	CVPR ₂₁	ResNet-50	0.804	0.673	0.037	0.883	0.880	0.892	0.699	0.715	0.732
R-MGL [116]	CVPR ₂₁	ResNet-50	0.814	0.666	0.035	0.865	0.852	0.890	0.681	0.711	0.738
S-MGL [116]	CVPR ₂₁	ResNet-50	0.811	0.655	0.037	0.851	0.845	0.889	0.667	0.702	0.733
PFNet [25]	CVPR ₂₁	ResNet-50	0.800	0.660	0.040	0.868	0.877	0.890	0.676	0.701	0.725
UGTR [117]	ICCV ₂₁	ResNet-50	0.818	0.667	0.035	0.850	0.853	0.891	0.671	0.712	0.742
BAS [118]	arXiv ₂₁	ResNet-34	0.802	0.677	0.038	0.869	0.855	0.870	0.707	0.715	0.729
NCHIT [119]	CVIU ₂₂	ResNet-50	0.792	0.591	0.046	0.794	0.819	0.879	0.596	0.649	0.698
C2FNet-V2 [121]	TCSVT ₂₂	Res2Net-50	0.811	0.691	0.036	0.890	0.887	0.896	0.718	0.725	0.742
CubeNet [122]	PR ₂₂	ResNet-50	0.795	0.643	0.041	0.862	0.865	0.883	0.669	0.692	0.715
ERRNet [123]	PR ₂₂	ResNet-50	0.786	0.630	0.043	0.845	0.867	0.886	0.646	0.675	0.702
TPRNet [124]	TVCJ ₂₂	Res2Net-50	0.817	0.683	0.036	0.869	0.887	0.903	0.694	0.724	0.748
FAPNet [127]	TIP ₂₂	Res2Net-50	0.822	0.694	0.036	0.875	0.888	0.902	0.707	0.731	0.758
BSANet [126]	AAAI ₂₂	Res2Net-50	0.818	0.699	0.034	0.894	0.891	0.901	0.723	0.738	0.753
OCENet [130]	WACV ₂₂	ResNet-50	0.827	0.707	0.033	0.885	0.894	0.905	0.718	0.741	0.764
BGNet [131]	IJCAI ₂₂	Res2Net-50	0.831	0.722	0.033	0.902	0.901	0.911	0.739	0.753	0.774
PreyNet [132]	MM ₂₂	ResNet-50	0.813	0.697	0.034	0.894	0.881	0.891	0.731	0.736	0.747
ZoomNet [134]	CVPR ₂₂	ResNet-50	0.838	0.729	0.029	0.893	0.888	0.911	0.741	0.766	0.780
FDNet [135]	CVPR ₂₂	Res2Net-50	0.840	0.729	0.030	0.906	0.919	0.935	0.728	0.757	0.788
SegMaR [136]	CVPR ₂₂	ResNet-50	0.833	0.724	0.034	0.893	0.899	0.906	0.739	0.757	0.774
SINetV2 [22]	TPAMI ₂₂	Res2Net-50	0.815	0.680	0.037	0.864	0.887	0.906	0.682	0.718	0.752
CamoFormer-C [146]	arXiv ₂₃	ConvNeXt-B	0.860	0.770	0.024	0.926	0.926	0.935	0.778	0.798	0.818
CamoFormer-R [146]	arXiv ₂₃	ResNet-50	0.838	0.724	0.029	0.900	0.916	0.930	0.721	0.753	0.786
PopNet [147]	arXiv ₂₃	Res2Net-50	0.851	0.757	0.028	0.910	0.910	0.919	0.771	0.786	0.802
CRNet [142]	AAAI ₂₃	ResNet-50	0.733	0.576	0.049	0.845	0.832	0.845	0.637	0.633	0.636
PFNet+ [26]	Ssis ₂₃	ResNet-50	0.806	0.677	0.037	0.880	0.884	0.895	0.698	0.716	0.734
DGNet-S [28]	MIR ₂₃	EfficientNet-B1	0.810	0.672	0.036	0.869	0.888	0.905	0.680	0.710	0.743
DGNet [28]	MIR ₂₃	EfficientNet-B4	0.822	0.693	0.033	0.879	0.896	0.911	0.698	0.728	0.759
• Transformer-based Backbone											
DTINet [133]	ICPR ₂₂	MiT-B5	0.824	0.695	0.034	0.881	0.896	0.911	0.702	0.726	0.754
CamoFormer-S [146]	arXiv ₂₃	Swin-B	0.862	0.772	0.024	0.932	0.931	0.941	0.780	0.799	0.818
CamoFormer-P [146]	arXiv ₂₃	PVTv2-B4	0.869	0.786	0.023	0.931	0.932	0.939	0.794	0.811	0.829
HitNet [143]	AAAI ₂₃	PVTv2-B2	0.871	0.806	0.023	0.936	0.935	0.938	0.818	0.823	0.838

better than two other competitors (*i.e.*, SegMaR [136] and ZoomNet [134]) on NC4K. These results confirm the effectiveness of CamoFormer’s decoder design in mapping latent features back to the prediction space, particularly for more complicated scenarios.

- DGNet [28] shows less promise on the challenging NC4K dataset, possibly due to its restricted modeling capability with small model parameters. Nevertheless, this drawback provides an opening for modification since the model has a lightweight and simple architecture.

- While PopNet [147] may not perform well on small-scale CMAO datasets, it has demonstrated potential in challenging NC4K dataset. This indicates that using extra network to synthesize depth priors would be helpful for challenging samples. When compared to SINetV2 based on Res2Net-50 [22], PopNet has a heavier design (188.05M *vs.* 26.98M) and larger input resolution (512^2 *vs.* 352^2), but only improves the E_ϕ^{mn} value by 0.6%.

- Regarding the CamoFormer [146] model, there is now a noticeable difference in performance between its two variants. Specifically, the CamoFormer-S variant based on Swin-B lags behind while the CamoFormer-P variant based on PVTv2-B4 performs better.

5.5 Quantitative Analysis on COD10K

In Table 6, we present a performance comparison of 36 competitors, including 32 convolutional-based models and four transformer-based models, on the COD10K dataset with diverse concealed samples. Based on our evaluation, we have made the following observations:

- CamoFormer-C [146], which has a robust backbone, remains the best-performing method among all convolutional-based methods. Similarly to its performance on NC4K, CamoFormer-R [146] has once again outperformed strong competitors with identical backbones such as SegMaR [136] and ZoomNet [134].

- Similar to its performance on the NC4K dataset, PopNet [147] achieves consistently high results on the COD10K dataset, ranking second only to CamoFormer-C [146]. We believe that prior knowledge of the depth of the scene plays a crucial role in enhancing the understanding of concealed environments. This insight will motivate us to investigate more intelligent ways to learn structural priors, such as incorporating multi-task learning or heuristic methods into our models.

- Notably, HitNet [143] achieves the highest performance on the COD10K benchmark, outperforming models with stronger backbones like Swin-B and PVTv2-B4. To understand why this is the case, we calculated the average resolution of all samples in the CAMO ($W=693.89$ and $H=564.22$), NC4K ($W=709.19$ and $H=529.61$), and COD10K ($W=963.34$ and $H=740.54$) datasets. We found that the testing set for COD10K has the highest overall resolution, which suggests that models utilizing higher resolutions or multi-scale modeling would benefit from this characteristic. Therefore, HitNet is an excellent choice for detecting concealed objects in scenarios where high-resolution images are available.

5.6 Qualitative Comparison

This section visually assesses the performance of current top models on challenging and complex samples that are prone to

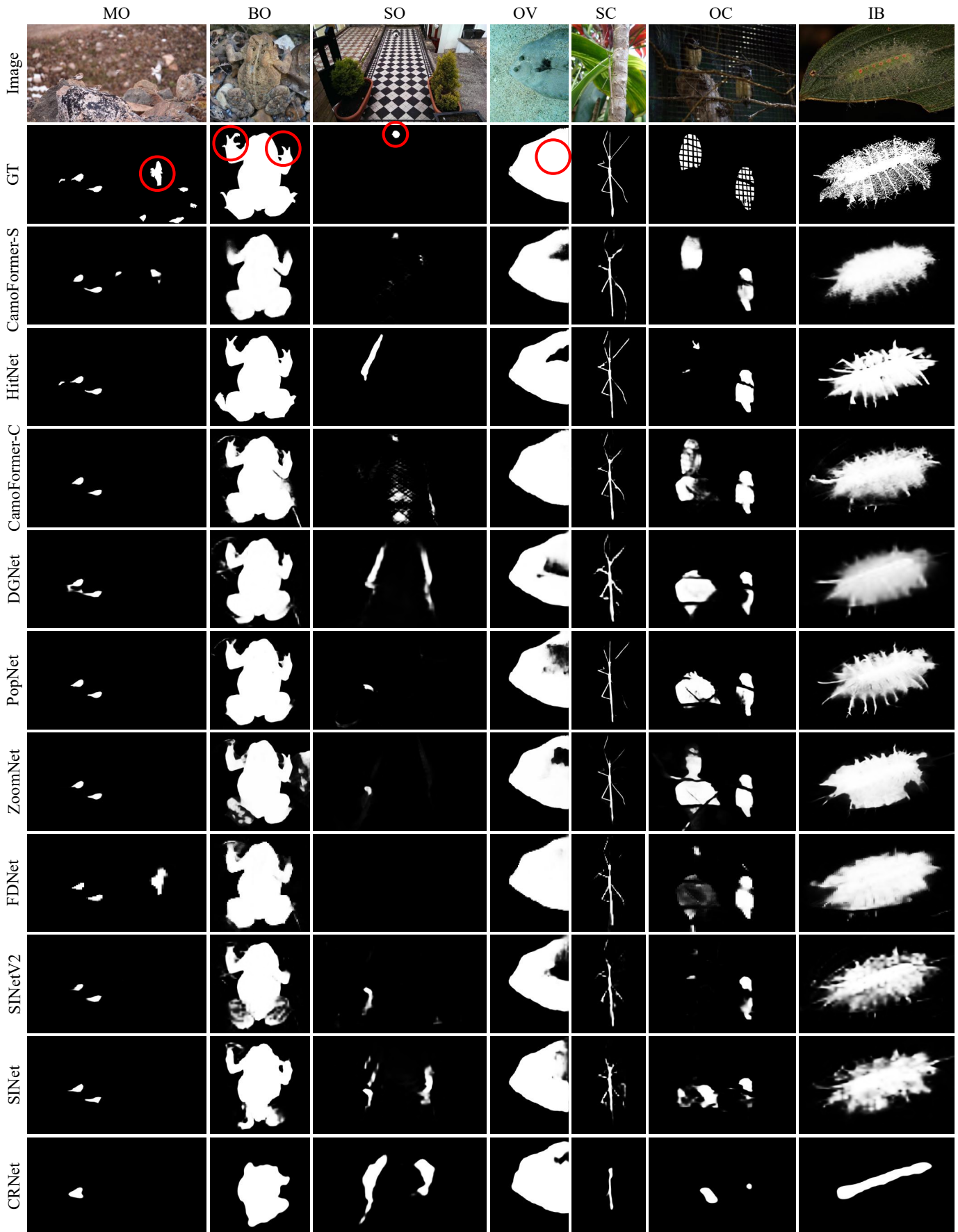


Fig. 4. Qualitative results of ten COS approaches. More descriptions on visual attributes in each column refer to §5.6.

failure. We compare qualitative results predicted by ten groups of top-performing models, including six convolutional-based models (*i.e.*, CamoFormer-C [146], DGNNet [28], PopNet [147], ZoomNet [134], FDNNet [135] and SINetV2 [22]), two transformer-based models (*i.e.*, CamoFormer-S [146] and HitNet [143]), as well as two other competitors (*i.e.*, the earliest baseline SINet [19] and a weakly-supervised model CRNet [142]). All samples are selected from the COD10K testing dataset according to seven fine-grained attributes. The qualitative comparison is presented in Fig. 4, revealing several interesting findings.

- The attribute of multiple objects (MO) poses a challenge due to the high false-negative rate in current top-performing models. As depicted in the first column of Fig. 4, only two out of ten models could locate the white flying bird approximately, as indicated by the red circle in the GT mask. These two models are CamoFormer-S [146], which employs a robust transformer-based encoder, and FDNNet [135], which utilizes a frequency domain learning strategy.
- The models we tested can accurately detect big objects (BO) by precisely locating the target’s main part. However, these models struggle to identify smaller details such as the red circles highlighting the toad’s claws in the second column of Fig. 4.
- Small object (SO) attribute presents a challenge as it only occupies a small area in the image, typically less than 10% of the total pixels as reported by COD10K [19]. As shown in the third column of Fig. 4, only two models (CamoFormer-S and CamoFormer-C [146]) can detect a cute cat lying on the ground in the distance. Such a difficulty arises for two main reasons: firstly, models struggle to differentiate small objects from complex backgrounds or other irrelevant objects in an image; secondly, detectors may miss small regions due to down-sampling operations caused by low-resolution inputs.
- Out-of-view (OV) attribute refers to objects partially outside the image boundaries, leading to incomplete representation. To address this issue, a model should have a better holistic understanding of the concealed scene. As shown in the fourth column of Figure 4, both CamoFormer-C [146] and FDNNet [135] can handle the OV attribute and maintain the object’s integrity. However, two transformer-based models failed to do so. This observation has inspired us to explore more efficient methods, such as local modeling within convolutional based frameworks and cross-domain learning strategies.
- Shape complexity (SC) attribute indicates that an object contains thin parts, such as an animal’s foot. In the fifth column of Fig. 4, the stick insect’s feet are a good example of this complexity, being elongated and slender and thus difficult to predict accurately. Only HitNet [143] with high-resolution inputs can predict a right-bottom foot (indicated by a red circle).
- The attribute of occlusion (OC) refers to the partial occlusion of objects, which is a common challenge in general scenes [182]. In Fig. 4, for example, the sixth column shows two owls partially occluded by a wire fence, causing their visual regions to be separated. Unfortunately, most of the models presented were unable to handle such cases.
- Indefinable boundary (IB) attribute is hard to address since its uncertainty between foreground and background. As shown in the last column of Fig. 4, a matting-level sample.
- In the last two rows of Fig. 4, we display the predictions generated by SINet [19], which was our earliest baseline model. Current models have significantly improved location accuracy, boundary details, and other aspects. Additionally, CRNet [142],

a weakly-supervised method with only weak label supervision, can effectively locate target objects to meet satisfactory standards.

6 DISCUSSION AND OUTLOOK

Based on our literature review and experimental analyses, we discuss five challenges and potential CSU-related directions in this section.

Annotation-Efficient Learning. Deep learning techniques have significantly advanced the field of CSU. However, conventional supervised deep learning is data-hungry and resource-consuming. In practical scenarios, we hope the models can work on limited resources and have good transferability. Thus developing effective learning strategies for CSU tasks is a promising direction, *e.g.*, weakly-supervised strategy in CRNet [142].

Domain Adaptation. Camouflaged samples are generally collected from natural scenes. Thus, deploying the models to detect concealed objects in auto-driving scenarios is challenging. Recent practice demonstrates that various techniques can be used to alleviate this problem, *e.g.*, domain adaptation [183], transfer learning [184], few-shot learning [185], and meta-learning [186].

High-Fidelity Synthetic Dataset. To alleviate algorithmic biases, increasing the diversity and scale of data is crucial. The rapid development of AI-generated content (AIGC) [187] and deep generative models, such as generative adversarial networks [188], [189], [190] and diffusion models [191], [192], is making it easier to create synthetic data for general domains. Recently, to address the scarcity of multi-pattern training images, Luo *et al.* [107] proposed a diffusion-based image generation framework that generates salient objects on a camouflaged sample while preserving its original label. Therefore, a model should be capable of distinguishing between camouflaged and salient objects to achieve a robust feature representation.

Neural Architecture Search. Automatic network architecture search (NAS) is a promising research direction that can discover optimal network architectures for superior performance on a given task. In the context of concealment, NAS can identify more effective network architectures to handle complex background scenes, highly variable object appearances, and limited labeled data. This can lead to the developing of more efficient and effective network architectures, resulting in improved accuracy and efficiency. Combining NAS with other research directions, such as domain adaptation and data-efficient learning, can further enhance the understanding of concealed scenes. These avenues of exploration hold significant potential for advancing the state-of-the-art and warrant further investigation in future research.

Large Model and Prompt Engineering. This topic has gained popularity and has even become a direction for the natural language processing community. Recently, the Segment Anything Model (SAM) [193] has revolutionized computer vision algorithms, although it has limitations [194] in unprompted settings on several concealed scenarios. One can leverage the prompt engineering paradigm to simplify workflows using a well-trained robust encoder and task-specific adaptations, such as task-specific prompts and multi-task prediction heads. This approach is expected to become a future trend within the computer vision community. Large language models (LLMs) have brought both new opportunities and challenges to AI, moving towards artificial general intelligence further. However, it is challenging for

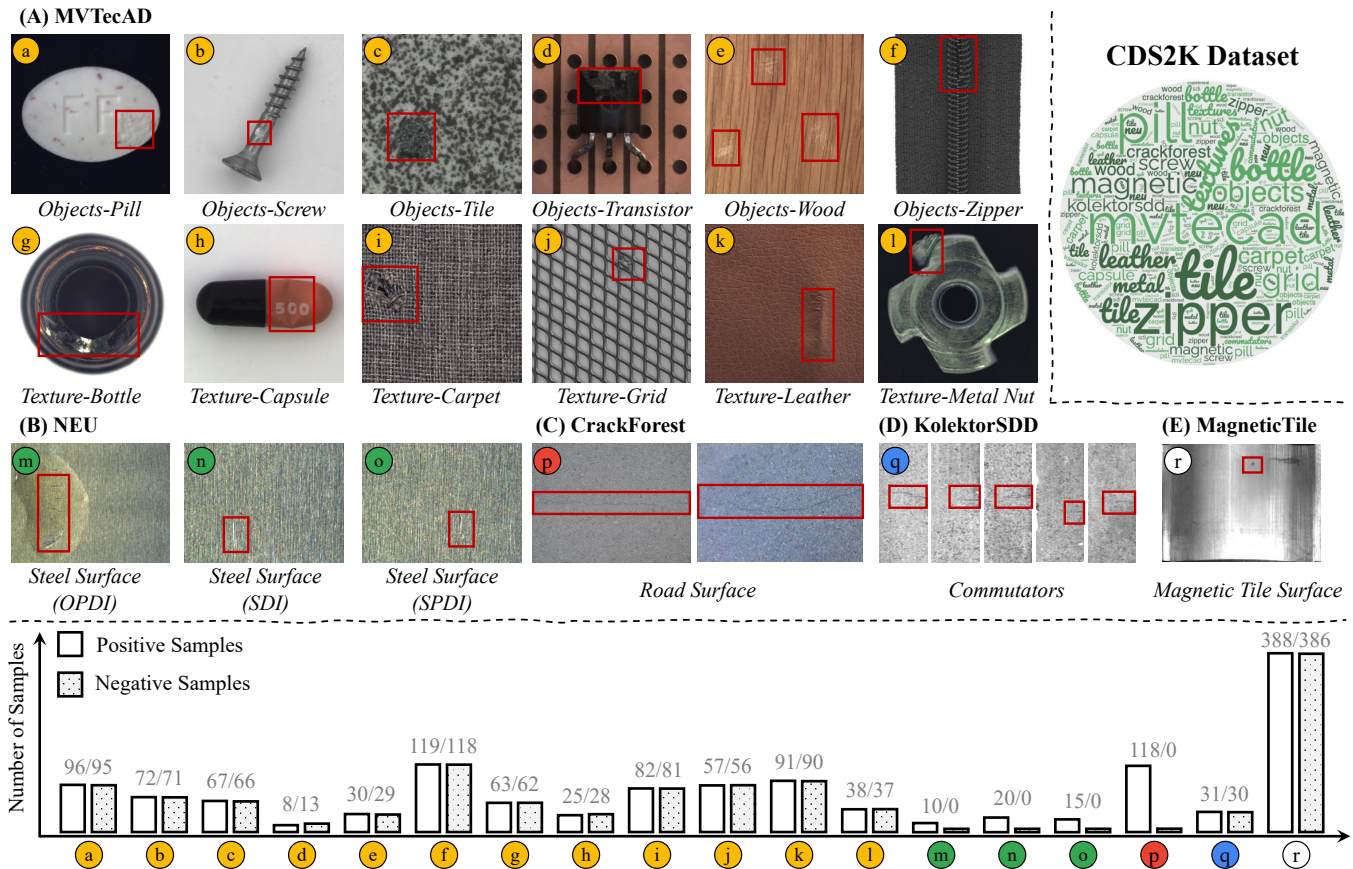


Fig. 5. **Sample gallery of our CDS2K.** It is collected from five sub-databases: (a-l) MVTecAD, (m-o) NEU, (p) CrackForest, (q) KolektorSDD, and (r) MagneticTile. The defective regions are highlighted with red rectangles. (Top-Right) Word cloud visualization of CDS2K. (Bottom) The statistic number of positive/negative samples of each category in our CDS2K.

academia to train the resource-consuming large models. There could be a promising paradigm that the state-of-the-art deep CSU models are used as the domain experts, and meanwhile, the large models could work as an external component to assist the expert models by providing an auxiliary decision, representation, *etc*

7 DEFECT SEGMENTATION DATASET

Industrial defects usually originate from the undesirable production process, *e.g.*, mechanical impact, workpiece friction, chemical corrosion, and other unavoidable physical, whose external visual form is usually with unexpected patterns or outliers, *e.g.*, surface scratches, spots, holes on industrial devices; color difference, indentation on fabric surface; impurities, breakage, stains on the material surface, *etc* Though previous works achieve promising advances for identifying visual defects by vision-based techniques, such as classification [195], [196], [197], detection [198], [199], [200], and segmentation [201], [202], [203]. These techniques work on the assumption that defects are easily detected, but they ignore those challenging defects that are “seamlessly” embedded in their materials surroundings. With this, we elaborately re-organise a new multi-scene benchmark, named CDS2K, for the concealed defect segmentation task, whose samples are selected from existing industrial defect databases.

7.1 Dataset Organisation

To create a dataset of superior quality, we established three principles for selecting data: (a) The chosen sample should include

at least one defective region, which will serve as a positive example. (b) The defective regions should have a pattern similar to the background, making them difficult to identify. (c) We also select normal cases as negative examples to provide a contrasting perspective with the positive ones. These samples were selected from the following well-known defect segmentation databases.

- MVTecAD⁴ [204], [205] contains several positive and negative samples for unsupervised anomaly detection. We manually select 748 positive and 746 negative samples with concealed patterns from two main categories: (a) object category as in the 1st row of Fig. 5: pill, screw, tile, transistor, wood, and zipper. (b) texture category as in the 2nd row of Fig. 5: bottle, capsule, carpet, grid, leather, and metal nut. The number of positive/negative samples is shown with yellow circles in Fig. 5

- NEU⁵ provides three different database: oil pollution defect images [206] (OPDI), spot defect images [207] (SDI), and steel pit defect images [208] (SPDI). As shown in the third row (green circles) of Fig. 5, we select 10, 20, and 15 positive samples from these databases separately.

- CrackForest⁶ [209], [210] is a densely-annotated road crack image database for the health monitoring of urban road surface. We select 118 samples with concealed patterns from them, and the samples are shown in the third row (red circle) of Fig. 5.

4. <https://www.mvtec.com/company/research/datasets/mvtec-ad>

5. http://faculty.neu.edu.cn/songkechen/zh_CN/zdylm/263270/list/index.htm

6. <https://github.com/cuilimeng/CrackForest-dataset>

TABLE 7

Statistic of positive samples in CDS2K. The region ratio is calculated by $r = \text{defective pixels} / \text{all pixels}$ for a given image. Of note, we only count the number of positive samples in five sub-datasets.

Category		$0\% < r < 1\%$	$1\% \leq r < 10\%$	$10\% \leq r < 20\%$	$20\% \leq r < 30\%$	$30\% \leq r < 40\%$	$40\% \leq r < 50\%$	Total
MVTecAD	Objects-Pill	41	55	0	0	0	0	96
	Objects-Screw	71	1	0	0	0	0	72
	Objects-Tile	0	30	28	7	2	0	67
	Objects-Transistor	1	7	0	0	0	0	8
	Objects-Wood	2	26	2	0	0	0	30
	Objects-Zipper	16	102	1	0	0	0	119
	Texture-Bottle	3	39	20	1	0	0	63
	Texture-Capsule	17	8	0	0	0	0	25
	Texture-Carpet	37	45	0	0	0	0	82
	Texture-Grid	39	18	0	0	0	0	57
	Texture-Leather	70	21	0	0	0	0	91
	Texture-Metal Nut	6	31	1	0	0	0	38
NEU	OPDI	10	0	0	0	0	0	10
	SDI	20	0	0	0	0	0	20
	SPDI	15	0	0	0	0	0	15
	CrackForest	28	90	0	0	0	0	118
KolektorSDD		31	0	0	0	0	0	31
Magnetic Tile Defect		216	70	27	27	24	24	388
Total		623	543	79	35	26	24	1330

TABLE 8

Quantitative comparison on the positive samples of CDS2K.

Model	Pub/Year	Backbone	$S_\alpha \uparrow$	$F_\beta^w \uparrow$	$M \downarrow$	$E_\phi^{ad} \uparrow$	$E_\phi^{mn} \uparrow$	$E_\phi^{mx} \uparrow$	$F_\beta^{ad} \uparrow$	$F_\beta^{mn} \uparrow$	$F_\beta^{mx} \uparrow$
SINetV2 [22]	TPAMI ₂₂	Res2Net-50	0.551	0.215	0.102	0.509	0.567	0.597	0.223	0.248	0.258
HitNet [143]	AAAI ₂₃	PVTv2-B2	0.563	0.276	0.118	0.574	0.564	0.570	0.298	0.298	0.299
DGNet [28]	MIR ₂₃	EfficientNet-B4	0.578	0.258	0.089	0.552	0.569	0.579	0.274	0.291	0.297
CamoFormer-P [146]	arXiv ₂₃	PVTv2-B4	0.589	0.298	0.100	0.590	0.588	0.596	0.330	0.329	0.339

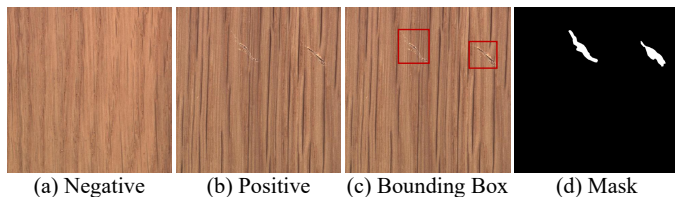


Fig. 6. **Visualization of different annotations.** We select a group of images from the MVTecAD database, including a negative (a) and a positive (b) sample. Corresponding annotations are provided: category (scratches on wood) and defect locations: bounding box (c) and segmentation mask (d).

- KolektorSDD⁷ [202] collected and annotated by Kolektor Group, which contains several non-defective surfaces from the controlled industrial environment in a real-world case. We manually select 31 positive and 30 negative samples with concealed patterns, and the positive samples are shown in the third row (blue circle) of Fig. 5.
- Magnetic Tile Defect⁸ [211] datasets contains six common magnetic tile defects and corresponding dense annotations. We picked 388 positive and 386 negative examples, displayed as white circles in Fig. 5.

7.2 Dataset Description

The CDS2K comprises 2,492 samples, consisting of 1,330 positive and 1,162 negative instances. Three different human-annotated labels are provided to each sample – category, bounding box, and pixel-wise segmentation mask. Fig. 6 illustrates examples of these annotations. The average ratio of defective regions for each

category is presented in Table 7, which indicates that most of the defective regions are relatively small.

7.3 Evaluation on CDS2K

Here, we evaluate the generalizability of current cutting-edge COS models on the positive samples of CDS2K. Regarding the code availability, we here choose four top-performing COS approaches: SINetV2 [22], DGNet [28], CamoFormer-P [146], and HitNet [143]. As reported in Table 8, our observations indicate that these models are not effective in handling cross-domain samples, highlighting the need for further exploration of the domain gap between natural scene and downstream applications.

8 CONCLUSION

The purpose of this paper is to provide an overview of deep learning techniques tailored for concealed scene understanding (CSU). To help the readers view the global landscape of this field, we have made four contributions: Firstly, we provide a detailed survey of CSU, which includes its background, taxonomy, task-specific challenges, and advances in the deep learning era. To the best of our knowledge, this survey is the most comprehensive one to date. Secondly, we have created the largest and most up-to-date benchmark for concealed object segmentation (COS), which is a foundational and prosperous direction at CSU. This benchmark allows for a quantitative comparison of state-of-the-art techniques. Thirdly, we have reorganized the largest concealed defect segmentation dataset, CDS2K, by including hard cases from diverse industrial scenarios. We have also constructed a comprehensive benchmark to evaluate the generalizability of deep CSU in practical scenarios. Finally, we discuss open problems and potential directions for this community. We aim to encourage further research and development in this area.

7. <https://www.vicos.si/resources/kolektorsdd/>

8. <https://github.com/abin24/Magnetic-tile-defect-datasets>

We would conclude from the following perspectives. (1) **Model.** The most common practice is based on the architecture of sharing UNet, which is enhanced by various attention modules. In addition, injecting extra priors and/or introducing auxiliary tasks improve the performance, while there are many potential problems to explore. (2) **Training.** Fully-supervised learning is the mainstream strategy in COS, but few researchers have addressed the challenge caused by insufficient data or labels. CRNet [142] is a good attempt to alleviate this issue. (3) **Dataset.** The existing datasets are still not large and diverse enough. This community needs more concealed samples involving more domains (e.g., autonomous driving and clinical diagnosis). (4) **Performance.** Transformer and ConvNext based models outperform other competitors by a clear margin. Cost-performance tradeoff is still understudied, for which DGNNet [28] is a good attempt. (5) **Metric.** There is no well-defined metrics that can consider the different camouflage degree of different data to give a comprehensive evaluation. This causes unfair comparisons.

Besides, existing CSU methods focus on the appearance attributes of the concealed scenes (e.g., color, texture, boundary) to distinguish concealed objects without enough perception and output from the semantic perspective (e.g., relationships between objects). However, semantics is a good tool for bridging the human and machine intelligence gap. Therefore, beyond the visual space, semantic level awareness is key to the next-generation concealed visual perception. In the future, CSU models should incorporate various semantic abilities, including integrating high-level semantics, learning vision-language knowledge [212], and modeling interactions across objects.

We hope that this survey provides a detailed overview for new researchers presents a convenient reference for relevant experts, and encourages future research.

REFERENCES

- [1] D.-P. Fan, J. Zhang, G. Xu, M.-M. Cheng, and L. Shao, "Salient objects in clutter," *IEEE TPAMI*, vol. 45, no. 2, pp. 2344–2366, 2023.
- [2] H. Zhao, J. Shi, X. Qi, X. Wang, and J. Jia, "Pyramid scene parsing network," in *CVPR*, 2017.
- [3] G.-P. Ji, G. Xiao, Y.-C. Chou, D.-P. Fan, K. Zhao, G. Chen, and L. Van Gool, "Video polyp segmentation: A deep learning perspective," *MIR*, vol. 19, no. 6, p. 531–549, 2022.
- [4] D.-P. Fan, T. Zhou, G.-P. Ji, Y. Zhou, G. Chen, H. Fu, J. Shen, and L. Shao, "Inf-net: Automatic covid-19 lung infection segmentation from ct images," *IEEE TMI*, vol. 39, no. 8, pp. 2626–2637, 2020.
- [5] L. Liu, R. Wang, C. Xie, P. Yang, F. Wang, S. Sudirman, and W. Liu, "Pestnet: An end-to-end deep learning approach for large-scale multi-class pest detection and classification," *IEEE Access*, vol. 7, pp. 45 301–45 312, 2019.
- [6] M. Rizzo, M. Marcuzzo, A. Zangari, A. Gasparetto, and A. Albarelli, "Fruit ripeness classification: A survey," *AIA*, vol. 7, pp. 44–57, 2023.
- [7] H.-K. Chu, W.-H. Hsu, N. J. Mitra, D. Cohen-Or, T.-T. Wong, and T.-Y. Lee, "Camouflage images," *ACM TOG*, vol. 29, no. 4, pp. 51–1, 2010.
- [8] T. E. Boulton, R. J. Micheals, X. Gao, and M. Eckmann, "Into the woods: Visual surveillance of noncooperative and camouflaged targets in complex outdoor settings," *Proceedings of the IEEE*, vol. 89, no. 10, pp. 1382–1402, 2001.
- [9] D. Conte, P. Foggia, G. Percannella, F. Tufano, and M. Vento, "An algorithm for detection of partially camouflaged people," in *IEEE AVSS*, 2009.
- [10] J. Y. Y. H. W. Hou and J. Li, "Detection of the mobile object with camouflage color under dynamic background based on optical flow," *Procedia Engineering*, vol. 15, pp. 2201–2205, 2011.
- [11] S. Kim, "Unsupervised spectral-spatial feature selection-based camouflaged object detection using vnir hyperspectral camera," *TSWJ*, vol. 2015, 2015.
- [12] X. Zhang, C. Zhu, S. Wang, Y. Liu, and M. Ye, "A bayesian approach to camouflaged moving object detection," *IEEE TCSVT*, vol. 27, no. 9, pp. 2001–2013, 2016.
- [13] M. Galun, E. Sharon, R. Basri, and A. Brandt, "Texture segmentation by multiscale aggregation of filter responses and shape elements," in *ICCV*, 2003.
- [14] A. Tankus and Y. Yeshurun, "Detection of regions of interest and camouflage breaking by direct convexity estimation," in *IEEE WVS*, 1998.
- [15] —, "Convexity-based visual camouflage breaking," *CVIU*, vol. 82, no. 3, pp. 208–237, 2001.
- [16] A. Mittal and N. Paragios, "Motion-based background subtraction using adaptive kernel density estimation," in *CVPR*, 2004.
- [17] Z. Liu, K. Huang, and T. Tan, "Foreground object detection using top-down information based on em framework," *IEEE TIP*, vol. 21, no. 9, pp. 4204–4217, 2012.
- [18] S. Li, D. Florencio, Y. Zhao, C. Cook, and W. Li, "Foreground detection in camouflaged scenes," in *ICIP*, 2017.
- [19] D.-P. Fan, G.-P. Ji, G. Sun, M.-M. Cheng, J. Shen, and L. Shao, "Camouflaged object detection," in *CVPR*, 2020.
- [20] T.-N. Le, T. V. Nguyen, Z. Nie, M.-T. Tran, and A. Sugimoto, "Anabran network for camouflaged object segmentation," *CVIU*, vol. 184, pp. 45–56, 2019.
- [21] Q. Zhang, G. Yin, Y. Nie, and W.-S. Zheng, "Deep camouflage images," in *AAAI*, 2020.
- [22] D.-P. Fan, G.-P. Ji, M.-M. Cheng, and L. Shao, "Concealed object detection," *IEEE TPAMI*, vol. 44, no. 10, pp. 6024–6042, 2022.
- [23] Y. Lv, J. Zhang, Y. Dai, A. Li, B. Liu, N. Barnes, and D.-P. Fan, "Simultaneously localize, segment and rank the camouflaged objects," in *CVPR*, 2021.
- [24] M. W. Eysenck and C. Eysenck, *AI vs Humans*. Routledge, 2021.
- [25] H. Mei, G.-P. Ji, Z. Wei, X. Yang, X. Wei, and D.-P. Fan, "Camouflaged object segmentation with distraction mining," in *CVPR*, 2021.
- [26] H. Mei, X. Yang, Y. Zhou, G.-P. Ji, X. Wei, and D.-P. Fan, "Distraction-aware camouflaged object segmentation," *SCIS*, 2023.
- [27] L. Yu, H. Mei, W. Dong, Z. Wei, L. Zhu, Y. Wang, and X. Yang, "Progressive glass segmentation," *IEEE TIP*, vol. 31, pp. 2920–2933, 2022.
- [28] G.-P. Ji, D.-P. Fan, Y.-C. Chou, D. Dai, A. Liniger, and L. Van Gool, "Deep gradient learning for efficient camouflaged object detection," *MIR*, vol. 20, pp. 92–108, 2023.
- [29] J. S. Kulchandani and K. J. Dangarwala, "Moving object detection: Review of recent research trends," in *IEEE ICPC*, 2015.
- [30] A. Mondal, "Camouflaged object detection and tracking: A survey," *IJIG*, vol. 20, no. 04, p. 2050028, 2020.
- [31] H. Bi, C. Zhang, K. Wang, J. Tong, and F. Zheng, "Rethinking camouflaged object detection: Models and datasets," *IEEE TCSVT*, vol. 32, no. 9, pp. 5708–5724, 2022.
- [32] S. Caijuan, R. Bijuan, W. Ziwen, Y. Jinwei, and S. Ze, "Survey of camouflaged object detection based on deep learning," *IFCST*, vol. 16, no. 12, p. 2734, 2022.
- [33] Y. Lv, J. Zhang, Y. Dai, A. Li, N. Barnes, and D.-P. Fan, "Towards deeper understanding of camouflaged object detection," *IEEE TCSVT*, 2023.
- [34] K. He, G. Gkioxari, P. Dollár, and R. Girshick, "Mask r-cnn," in *ICCV*, 2017.
- [35] J. Pei, T. Cheng, D.-P. Fan, H. Tang, C. Chen, and L. Van Gool, "Osformer: One-stage camouflaged instance segmentation with transformers," in *ECCV*, 2022.
- [36] T.-N. Le, Y. Cao, T.-C. Nguyen, M.-Q. Le, K.-D. Nguyen, T.-T. Do, M.-T. Tran, and T. V. Nguyen, "Camouflaged instance segmentation in-the-wild: Dataset, method, and benchmark suite," *IEEE TIP*, vol. 31, pp. 287–300, 2022.
- [37] E. Xie, W. Wang, M. Ding, R. Zhang, and P. Luo, "Polarmask++: Enhanced polar representation for single-shot instance segmentation and beyond," *IEEE TPAMI*, vol. 44, no. 9, pp. 5385–5400, 2021.
- [38] H. Chen, K. Sun, Z. Tian, C. Shen, Y. Huang, and Y. Yan, "Blendmask: Top-down meets bottom-up for instance segmentation," in *CVPR*, 2020.
- [39] G. Sun, Z. An, Y. Liu, C. Liu, C. Sakaridis, D.-P. Fan, and L. Van Gool, "Indiscernible object counting in underwater scenes," in *CVPR*, 2023.
- [40] H. Lamdouar, C. Yang, W. Xie, and A. Zisserman, "Betrayed by motion: Camouflaged object discovery via motion segmentation," in *ACCV*, 2020.
- [41] L. Jiao, R. Zhang, F. Liu, S. Yang, B. Hou, L. Li, and X. Tang, "New generation deep learning for video object detection: A survey," *IEEE TNLS*, vol. 33, no. 8, pp. 3195–3215, 2022.
- [42] X. Cheng, H. Xiong, D.-P. Fan, Y. Zhong, M. Harandi, T. Drummond, and Z. Ge, "Implicit motion handling for video camouflaged object detection," in *CVPR*, 2022.

- [43] D.-P. Fan, M.-M. Cheng, J.-J. Liu, S.-H. Gao, Q. Hou, and A. Borji, "Salient objects in clutter: Bringing salient object detection to the foreground," in *ECCV*, 2018.
- [44] S. He, R. W. Lau, W. Liu, Z. Huang, and Q. Yang, "Supercnn: A superpixelwise convolutional neural network for salient object detection," *IJCV*, vol. 115, no. 3, pp. 330–344, 2015.
- [45] G. Li and Y. Yu, "Visual saliency based on multiscale deep features," in *CVPR*, 2015.
- [46] L. Wang, H. Lu, X. Ruan, and M.-H. Yang, "Deep networks for saliency detection via local estimation and global search," in *CVPR*, 2015.
- [47] J. Kim and V. Pavlovic, "A shape-based approach for salient object detection using deep learning," in *ECCV*, 2016.
- [48] Y. Zeng, P. Zhang, J. Zhang, Z. Lin, and H. Lu, "Towards high-resolution salient object detection," in *ICCV*, 2019.
- [49] N. Liu and J. Han, "Dhsnet: Deep hierarchical saliency network for salient object detection," in *CVPR*, 2016.
- [50] Z. Wu, L. Su, and Q. Huang, "Cascaded partial decoder for fast and accurate salient object detection," in *CVPR*, 2019.
- [51] P. Zhang, D. Wang, H. Lu, H. Wang, and B. Yin, "Learning uncertain convolutional features for accurate saliency detection," in *ICCV*, 2017.
- [52] Q. Hou, M.-M. Cheng, X. Hu, A. Borji, Z. Tu, and P. H. S. Torr, "Deeply supervised salient object detection with short connections," *IEEE TPAMI*, vol. 41, no. 4, pp. 815–828, 2019.
- [53] M. Zhuge, D.-P. Fan, N. Liu, D. Zhang, D. Xu, and L. Shao, "Salient object detection via integrity learning," *IEEE TPAMI*, vol. 45, no. 3, pp. 3738–3752, 2023.
- [54] Y. Liu, Q. Zhang, D. Zhang, and J. Han, "Employing deep part-object relationships for salient object detection," in *ICCV*, 2019.
- [55] Q. Qi, S. Zhao, J. Shen, and K.-M. Lam, "Multi-scale capsule attention-based salient object detection with multi-crossed layer connections," in *ICME*, 2019.
- [56] N. Liu, N. Zhang, K. Wan, L. Shao, and J. Han, "Visual saliency transformer," in *ICCV*, 2021.
- [57] G. Li and Y. Yu, "Deep contrast learning for salient object detection," in *CVPR*, 2016.
- [58] Y. Tang and X. Wu, "Saliency detection via combining region-level and pixel-level predictions with cnns," in *ECCV*, 2016.
- [59] L. Wang, H. Lu, Y. Wang, M. Feng, D. Wang, B. Yin, and X. Ruan, "Learning to detect salient objects with image-level supervision," in *CVPR*, 2017.
- [60] G. Li, Y. Xie, and L. Lin, "Weakly supervised salient object detection using image labels," in *AAAI*, 2018.
- [61] C. Cao, Y. Huang, Z. Wang, L. Wang, N. Xu, and T. Tan, "Lateral inhibition-inspired convolutional neural network for visual attention and saliency detection," in *AAAI*, 2018.
- [62] B. Li, Z. Sun, and Y. Guo, "Supervae: Superpixelwise variational autoencoder for salient object detection," in *AAAI*, 2019.
- [63] Y. Zeng, Y. Zhuge, H. Lu, L. Zhang, M. Qian, and Y. Yu, "Multi-source weak supervision for saliency detection," in *CVPR*, 2019.
- [64] D. Zhang, J. Han, and Y. Zhang, "Supervision by fusion: Towards unsupervised learning of deep salient object detector," in *ICCV*, 2017.
- [65] J. Zhang, T. Zhang, Y. Dai, M. Harandi, and R. Hartley, "Deep unsupervised saliency detection: A multiple noisy labeling perspective," in *CVPR*, 2018.
- [66] G. Shin, S. Albanie, and W. Xie, "Unsupervised salient object detection with spectral cluster voting," in *CVPR*, 2022.
- [67] S. He, J. Jiao, X. Zhang, G. Han, and R. W. Lau, "Delving into salient object subitizing and detection," in *ICCV*, 2017.
- [68] M. A. Islam, M. Kalash, and N. D. Bruce, "Revisiting salient object detection: Simultaneous detection, ranking, and subitizing of multiple salient objects," in *CVPR*, 2018.
- [69] W. Wang, J. Shen, X. Dong, and A. Borji, "Salient object detection driven by fixation prediction," in *CVPR*, 2018.
- [70] S. S. Kruthiventhi, V. Gudisa, J. H. Dholakiya, and R. V. Babu, "Saliency unified: A deep architecture for simultaneous eye fixation prediction and salient object segmentation," in *CVPR*, 2016.
- [71] Y. Zeng, Y. Zhuge, H. Lu, and L. Zhang, "Joint learning of saliency detection and weakly supervised semantic segmentation," in *ICCV*, 2019.
- [72] L. Wang, L. Wang, H. Lu, P. Zhang, and X. Ruan, "Saliency detection with recurrent fully convolutional networks," in *ECCV*, 2016.
- [73] X. Li, F. Yang, H. Cheng, W. Liu, and D. Shen, "Contour knowledge transfer for salient object detection," in *ECCV*, 2018.
- [74] W. Wang, S. Zhao, J. Shen, S. C. Hoi, and A. Borji, "Salient object detection with pyramid attention and salient edges," in *CVPR*, 2019.
- [75] J.-J. Liu, Q. Hou, M.-M. Cheng, J. Feng, and J. Jiang, "A simple pooling-based design for real-time salient object detection," in *CVPR*, 2019.
- [76] J.-X. Zhao, J.-J. Liu, D.-P. Fan, Y. Cao, J. Yang, and M.-M. Cheng, "Egnet: Edge guidance network for salient object detection," in *ICCV*, 2019.
- [77] J. Su, J. Li, Y. Zhang, C. Xia, and Y. Tian, "Selectivity or invariance: Boundary-aware salient object detection," in *ICCV*, 2019.
- [78] L. Zhang, J. Zhang, Z. Lin, H. Lu, and Y. He, "Capsal: Leveraging captioning to boost semantics for salient object detection," in *CVPR*, 2019.
- [79] G. Li, Y. Xie, L. Lin, and Y. Yu, "Instance-level salient object segmentation," in *CVPR*, 2017.
- [80] X. Tian, K. Xu, X. Yang, B. Yin, and R. W. Lau, "Learning to detect instance-level salient objects using complementary image labels," *IJCV*, vol. 130, no. 3, pp. 729–746, 2022.
- [81] R. Fan, M.-M. Cheng, Q. Hou, T.-J. Mu, J. Wang, and S.-M. Hu, "S4net: Single stage salient-instance segmentation," in *CVPR*, 2019.
- [82] Y.-H. Wu, Y. Liu, L. Zhang, W. Gao, and M.-M. Cheng, "Regularized densely-connected pyramid network for salient instance segmentation," *IEEE TIP*, vol. 30, pp. 3897–3907, 2021.
- [83] A. Borji and L. Itti, "State-of-the-art in visual attention modeling," *IEEE TPAMI*, vol. 35, no. 1, pp. 185–207, 2012.
- [84] A. Borji, "Saliency prediction in the deep learning era: Successes and limitations," *IEEE TPAMI*, vol. 43, no. 2, pp. 679–700, 2019.
- [85] D.-P. Fan, T. Li, Z. Lin, G.-P. Ji, D. Zhang, M.-M. Cheng, H. Fu, and J. Shen, "Re-thinking co-salient object detection," *IEEE TPAMI*, vol. 44, no. 8, pp. 4339–4354, 2022.
- [86] D.-P. Fan, Z. Lin, G.-P. Ji, D. Zhang, H. Fu, and M.-M. Cheng, "Taking a deeper look at co-salient object detection," in *CVPR*, 2020.
- [87] D. Zhang, H. Fu, J. Han, A. Borji, and X. Li, "A review of co-saliency detection algorithms: fundamentals, applications, and challenges," *ACM TIST*, vol. 9, no. 4, pp. 1–31, 2018.
- [88] A. Borji, M.-M. Cheng, Q. Hou, H. Jiang, and J. Li, "Salient object detection: A survey," *CVMI*, vol. 5, no. 2, pp. 117–150, 2019.
- [89] W. Wang, Q. Lai, H. Fu, J. Shen, H. Ling, and R. Yang, "Salient object detection in the deep learning era: An in-depth survey," *IEEE TPAMI*, vol. 44, no. 6, pp. 3239–3259, 2021.
- [90] A. Borji, M.-M. Cheng, H. Jiang, and J. Li, "Salient object detection: A benchmark," *IEEE TIP*, vol. 24, no. 12, pp. 5706–5722, 2015.
- [91] T. Zhou, D.-P. Fan, M.-M. Cheng, J. Shen, and L. Shao, "Rgb-d salient object detection: A survey," *CVMI*, vol. 7, no. 1, pp. 37–69, 2021.
- [92] D.-P. Fan, Z. Lin, Z. Zhang, M. Zhu, and M.-M. Cheng, "Rethinking rgb-d salient object detection: Models, data sets, and large-scale benchmarks," *IEEE TNNLS*, vol. 32, no. 5, pp. 2075–2089, 2020.
- [93] R. Cong, K. Zhang, C. Zhang, F. Zhang, Y. Zhao, Q. Huang, and S. Kwong, "Does thermal really always matter for rgb-t salient object detection?" *IEEE TMM*, 2022.
- [94] Z. Tu, Z. Li, C. Li, Y. Lang, and J. Tang, "Multi-interactive dual-decoder for rgb-thermal salient object detection," *IEEE TIP*, vol. 30, pp. 5678–5691, 2021.
- [95] K. Fu, Y. Jiang, G.-P. Ji, T. Zhou, Q. Zhao, and D.-P. Fan, "Light field salient object detection: A review and benchmark," *CVMI*, pp. 1–26, 2022.
- [96] W. Wang, J. Shen, and L. Shao, "Video salient object detection via fully convolutional networks," *IEEE TIP*, vol. 27, no. 1, pp. 38–49, 2017.
- [97] T.-N. Le and A. Sugimoto, "Deeply supervised 3d recurrent fc for salient object detection in videos," in *BMVC*, 2017.
- [98] C. Chen, G. Wang, C. Peng, Y. Fang, D. Zhang, and H. Qin, "Exploring rich and efficient spatial temporal interactions for real-time video salient object detection," *IEEE TIP*, vol. 30, pp. 3995–4007, 2021.
- [99] T.-N. Le and A. Sugimoto, "Video salient object detection using spatiotemporal deep features," *IEEE TIP*, vol. 27, no. 10, pp. 5002–5015, 2018.
- [100] M. Zhang, J. Liu, Y. Wang, Y. Piao, S. Yao, W. Ji, J. Li, H. Lu, and Z. Luo, "Dynamic context-sensitive filtering network for video salient object detection," in *ICCV*, 2021.
- [101] G. Li, Y. Xie, T. Wei, K. Wang, and L. Lin, "Flow guided recurrent neural encoder for video salient object detection," in *CVPR*, 2018.
- [102] H. Song, W. Wang, S. Zhao, J. Shen, and K.-M. Lam, "Pyramid dilated deeper convlstm for video salient object detection," in *ECCV*, 2018.
- [103] G.-P. Ji, D.-P. Fan, K. Fu, Z. Wu, J. Shen, and L. Shao, "Full-duplex strategy for video object segmentation," *CVMI*, vol. 8, p. 155–175, 2022.
- [104] H. Li, G. Chen, G. Li, and Y. Yu, "Motion guided attention for video salient object detection," in *ICCV*, 2019.

- [105] R. Cong, W. Song, J. Lei, G. Yue, Y. Zhao, and S. Kwong, "Psnet: Parallel symmetric network for video salient object detection," *IEEE TETCI*, vol. 7, no. 2, pp. 402–414, 2023.
- [106] D.-P. Fan, W. Wang, M.-M. Cheng, and J. Shen, "Shifting more attention to video salient object detection," in *CVPR*, 2019.
- [107] X.-J. Luo, S. Wang, Z. Wu, C. Sakaridis, Y. Cheng, D.-P. Fan, and L. Van Gool, "Camdiff: Camouflage image augmentation via diffusion model," *arXiv preprint arXiv:2304.05469*, 2023.
- [108] A. Li, J. Zhang, Y. Lv, B. Liu, T. Zhang, and Y. Dai, "Uncertainty-aware joint salient object and camouflaged object detection," in *CVPR*, 2021.
- [109] X. Qin, H. Dai, X. Hu, D.-P. Fan, L. Shao, and L. Van Gool, "Highly accurate dichotomous image segmentation," in *ECCV*, 2022.
- [110] J. Yan, T.-N. Le, K.-D. Nguyen, M.-T. Tran, T.-T. Do, and T. V. Nguyen, "Mirrornet: Bio-inspired camouflaged object segmentation," *IEEE Access*, vol. 9, pp. 43 290–43 300, 2021.
- [111] M. Xiang, J. Zhang, Y. Lv, A. Li, Y. Zhong, and Y. Dai, "Exploring depth contribution for camouflaged object detection," *arXiv preprint arXiv:2106.13217*, 2021.
- [112] K. Wang, H. Bi, Y. Zhang, C. Zhang, Z. Liu, and S. Zheng, "D²c-net: A dual-branch, dual-guidance and cross-refine network for camouflaged object detection," *IEEE TIE*, vol. 69, no. 5, pp. 5364–5374, 2022.
- [113] Y. Sun, G. Chen, T. Zhou, Y. Zhang, and N. Liu, "Context-aware cross-level fusion network for camouflaged object detection," in *IJCAI*, 2021.
- [114] N. Kajiura, H. Liu, and S. Satoh, "Improving camouflaged object detection with the uncertainty of pseudo-edge labels," in *ACM MM Asia*, 2021.
- [115] J. Zhu, X. Zhang, S. Zhang, and J. Liu, "Inferring camouflaged objects by texture-aware interactive guidance network," in *AAAI*, 2021.
- [116] Q. Zhai, X. Li, F. Yang, C. Chen, H. Cheng, and D.-P. Fan, "Mutual graph learning for camouflaged object detection," in *CVPR*, 2021.
- [117] F. Yang, Q. Zhai, X. Li, R. Huang, A. Luo, H. Cheng, and D.-P. Fan, "Uncertainty-guided transformer reasoning for camouflaged object detection," in *ICCV*, 2021.
- [118] X. Qin, D.-P. Fan, C. Huang, C. Diagne, Z. Zhang, A. C. Sant'Anna, A. Suarez, M. Jagersand, and L. Shao, "Boundary-aware segmentation network for mobile and web applications," *arXiv preprint arXiv:2101.04704*, 2022.
- [119] C. Zhang, K. Wang, H. Bi, Z. Liu, and L. Yang, "Camouflaged object detection via neighbor connection and hierarchical information transfer," *CVIU*, vol. 221, p. 103450, 2022.
- [120] W. Zhai, Y. Cao, H. Xie, and Z.-J. Zha, "Deep texon-coherence network for camouflaged object detection," *IEEE TMM*, 2022.
- [121] G. Chen, S.-J. Liu, Y.-J. Sun, G.-P. Ji, Y.-F. Wu, and T. Zhou, "Camouflaged object detection via context-aware cross-level fusion," *IEEE TCSVT*, vol. 32, no. 10, pp. 6981–6993, 2022.
- [122] M. Zhuge, X. Lu, Y. Guo, Z. Cai, and S. Chen, "Cubenet: X-shape connection for camouflaged object detection," *PR*, vol. 127, p. 108644, 2022.
- [123] G.-P. Ji, L. Zhu, M. Zhuge, and K. Fu, "Fast camouflaged object detection via edge-based reversible re-calibration network," *PR*, vol. 123, p. 108414, 2022.
- [124] Q. Zhang, Y. Ge, C. Zhang, and H. Bi, "Tprnet: camouflaged object detection via transformer-induced progressive refinement network," *TVCI*, pp. 1–15, 2022.
- [125] Y. Cheng, H.-Z. Hao, Y. Ji, Y. Li, and C.-P. Liu, "Attention-based neighbor selective aggregation network for camouflaged object detection," in *IJCNN*, 2022.
- [126] H. Zhu, P. Li, H. Xie, X. Yan, D. Liang, D. Chen, M. Wei, and J. Qin, "I can find you! boundary-guided separated attention network for camouflaged object detection," in *AAAI*, 2022.
- [127] T. Zhou, Y. Zhou, C. Gong, J. Yang, and Y. Zhang, "Feature aggregation and propagation network for camouflaged object detection," *IEEE TIP*, vol. 31, pp. 7036–7047, 2022.
- [128] P. Li, X. Yan, H. Zhu, M. Wei, X.-P. Zhang, and J. Qin, "Findnet: Can you find me? boundary-and-texture enhancement network for camouflaged object detection," *IEEE TIP*, vol. 31, pp. 6396–6411, 2022.
- [129] M.-C. Chou, H.-J. Chen, and H.-H. Shuai, "Finding the achilles heel: Progressive identification network for camouflaged object detection," in *ICME*, 2022.
- [130] J. Liu, J. Zhang, and N. Barnes, "Modeling aleatoric uncertainty for camouflaged object detection," in *WACV*, 2022.
- [131] Y. Sun, S. Wang, C. Chen, and T.-Z. Xiang, "Boundary-guided camouflaged object detection," in *IJCAI*, 2022.
- [132] M. Zhang, S. Xu, Y. Piao, D. Shi, S. Lin, and H. Lu, "Preynet: Preying on camouflaged objects," in *ACM MM*, 2022.
- [133] Z. Liu, Z. Zhang, Y. Tan, and W. Wu, "Boosting camouflaged object detection with dual-task interactive transformer," in *ICPR*, 2022.
- [134] Y. Pang, X. Zhao, T.-Z. Xiang, L. Zhang, and H. Lu, "Zoom in and out: A mixed-scale triplet network for camouflaged object detection," in *CVPR*, 2022.
- [135] Y. Zhong, B. Li, L. Tang, S. Kuang, S. Wu, and S. Ding, "Detecting camouflaged object in frequency domain," in *CVPR*, 2022.
- [136] Q. Jia, S. Yao, Y. Liu, X. Fan, R. Liu, and Z. Luo, "Segment, magnify and reiterate: Detecting camouflaged objects the hard way," in *CVPR*, 2022.
- [137] Q. Zhai, X. Li, F. Yang, Z. Jiao, P. Luo, H. Cheng, and Z. Liu, "Mgl: Mutual graph learning for camouflaged object detection," *IEEE TIP*, vol. 32, pp. 1897–1910, 2023.
- [138] J. Lin, X. Tan, K. Xu, L. Ma, and R. W. Lau, "Frequency-aware camouflaged object detection," *ACM TMCCA*, vol. 19, no. 2, pp. 1–16, 2023.
- [139] J. Ren, X. Hu, L. Zhu, X. Xu, Y. Xu, W. Wang, Z. Deng, and P.-A. Heng, "Deep texture-aware features for camouflaged object detection," *IEEE TCSVT*, vol. 33, no. 3, pp. 1157–1167, 2023.
- [140] H. Xing, Y. Wang, X. Wei, H. Tang, S. Gao, and W. Zhang, "Go closer to see better: Camouflaged object detection via object area amplification and figure-ground conversion," *IEEE TCSVT*, 2023.
- [141] D. Zheng, X. Zheng, L. T. Yang, Y. Gao, C. Zhu, and Y. Ruan, "Mffn: Multi-view feature fusion network for camouflaged object detection," in *WACV*, 2023.
- [142] R. He, Q. Dong, J. Lin, and R. W. Lau, "Weakly-supervised camouflaged object detection with scribble annotations," in *AAAI*, 2023.
- [143] X. Hu, D.-P. Fan, X. Qin, H. Dai, W. Ren, Y. Tai, C. Wang, and L. Shao, "High-resolution iterative feedback network for camouflaged object detection," in *AAAI*, 2023.
- [144] Z. Huang, H. Dai, T.-Z. Xiang, S. Wang, H.-X. Chen, J. Qin, and H. Xiong, "Feature shrinkage pyramid for camouflaged object detection with transformers," in *CVPR*, 2023.
- [145] W. Sun, C. Liu, L. Zhang, Y. Li, P. Wei, C. Liu, J. Zou, J. Jiao, and Q. Ye, "Dqnet: Cross-model detail querying for camouflaged object detection," *arXiv preprint arXiv:2212.08296*, 2022.
- [146] B. Yin, X. Zhang, Q. Hou, B.-Y. Sun, D.-P. Fan, and L. Van Gool, "Camoforner: Masked separable attention for camouflaged object detection," *arXiv preprint arXiv:2212.06570*, 2023.
- [147] Z. Wu, D. P. Paudel, D.-P. Fan, J. Wang, S. Wang, C. Demonceaux, R. Timofte, and L. Van Gool, "Source-free depth for object pop-out," *arXiv preprint arXiv:2212.05370*, 2023.
- [148] J. Long, E. Shelhamer, and T. Darrell, "Fully convolutional networks for semantic segmentation," in *CVPR*, 2015.
- [149] S. Xie and Z. Tu, "Holistically-nested edge detection," in *ICCV*, 2015.
- [150] C.-Y. Lee, S. Xie, P. Gallagher, Z. Zhang, and Z. Tu, "Deeply-supervised nets," in *AISTATS*, 2015.
- [151] T.-Y. Lin, P. Dollár, R. Girshick, K. He, B. Hariharan, and S. Belongie, "Feature pyramid networks for object detection," in *CVPR*, 2017.
- [152] C. Xie, Y. Xiang, Z. Harchaoui, and D. Fox, "Object discovery in videos as foreground motion clustering," in *CVPR*, 2019.
- [153] H. Lamdouar, W. Xie, and A. Zisserman, "Segmenting invisible moving objects," in *BMVC*, 2021.
- [154] C. Yang, H. Lamdouar, E. Lu, A. Zisserman, and W. Xie, "Self-supervised video object segmentation by motion grouping," in *ICCV*, 2021.
- [155] P. Bideau, E. Learned-Miller, C. Schmid, and K. Alahari, "The right spin: Learning object motion from rotation-compensated flow fields," *arXiv preprint arXiv:2203.00115*, 2022.
- [156] J. Xie, W. Xie, and A. Zisserman, "Segmenting moving objects via an object-centric layered representation," in *NeurIPS*, 2022.
- [157] E. Meunier, A. Badoual, and P. Boutheymy, "Em-driven unsupervised learning for efficient motion segmentation," *IEEE TPAMI*, vol. 45, no. 4, pp. 4462–4473, 2023.
- [158] M. Koyal, M. Siam, M. A. Islam, N. D. Bruce, R. P. Wildes, and K. G. Derpanis, "A deeper dive into what deep spatiotemporal networks encode: Quantifying static vs. dynamic information," in *CVPR*, 2022.
- [159] F. Perazzi, J. Pont-Tuset, B. McWilliams, L. Van Gool, M. Gross, and A. Sorkine-Hornung, "A benchmark dataset and evaluation methodology for video object segmentation," in *CVPR*, 2016.
- [160] P. Ochs, J. Malik, and T. Brox, "Segmentation of moving objects by long term video analysis," *IEEE TPAMI*, vol. 36, no. 6, pp. 1187–1200, 2013.
- [161] P. Bideau and E. Learned-Miller, "It's moving! a probabilistic model for causal motion segmentation in moving camera videos," in *ECCV*, 2016.
- [162] L. Li, T. Zhou, W. Wang, L. Yang, J. Li, and Y. Yang, "Locality-aware inter-and intra-video reconstruction for self-supervised correspondence learning," in *CVPR*, 2022.

- [163] N. Araslanov, S. Schaub-Meyer, and S. Roth, “Dense unsupervised learning for video segmentation,” in *NeurIPS*, 2021.
- [164] R. Liu, Z. Wu, S. Yu, and S. Lin, “The emergence of objectness: Learning zero-shot segmentation from videos,” in *NeurIPS*, 2021.
- [165] X. Lu, W. Wang, J. Shen, Y.-W. Tai, D. J. Crandall, and S. C. Hoi, “Learning video object segmentation from unlabeled videos,” in *CVPR*, 2020.
- [166] M. Caron, H. Touvron, I. Misra, H. Jégou, J. Mairal, P. Bojanowski, and A. Joulin, “Emerging properties in self-supervised vision transformers,” in *ICCV*, 2021.
- [167] Z. Wang, H. Zhao, Y.-L. Li, S. Wang, P. Torr, and L. Bertinetto, “Do different tracking tasks require different appearance models?” in *NeurIPS*, 2021.
- [168] B. Yan, Y. Jiang, P. Sun, D. Wang, Z. Yuan, P. Luo, and H. Lu, “Towards grand unification of object tracking,” in *ECCV*, 2022.
- [169] H. Xu, J. Zhang, J. Cai, H. Rezatofighi, F. Yu, D. Tao, and A. Geiger, “Unifying flow, stereo and depth estimation,” *arXiv preprint arXiv:2211.05783*, 2022.
- [170] Z. Teed and J. Deng, “Raft: Recurrent all-pairs field transforms for optical flow,” in *ECCV*, 2020.
- [171] D.-P. Fan, G.-P. Ji, X. Qin, and M.-M. Cheng, “Cognitive vision inspired object segmentation metric and loss function,” *SCIS*, vol. 51, no. 9, pp. 1475–1489, 2021.
- [172] D.-P. Fan, C. Gong, Y. Cao, B. Ren, M.-M. Cheng, and A. Borji, “Enhanced-alignment measure for binary foreground map evaluation,” in *IJCAI*, 2018.
- [173] K. He, X. Zhang, S. Ren, and J. Sun, “Deep residual learning for image recognition,” in *CVPR*, 2016.
- [174] S.-H. Gao, M.-M. Cheng, K. Zhao, X.-Y. Zhang, M.-H. Yang, and P. Torr, “Res2net: A new multi-scale backbone architecture,” *IEEE TPAMI*, vol. 43, no. 2, pp. 652–662, 2019.
- [175] M. Tan and Q. Le, “Efficientnet: Rethinking model scaling for convolutional neural networks,” in *ICML*, 2019.
- [176] Z. Liu, H. Mao, C.-Y. Wu, C. Feichtenhofer, T. Darrell, and S. Xie, “A convnet for the 2020s,” in *CVPR*, 2022.
- [177] E. Xie, W. Wang, Z. Yu, A. Anandkumar, J. M. Alvarez, and P. Luo, “Segformer: Simple and efficient design for semantic segmentation with transformers,” in *NeurIPS*, 2021.
- [178] W. Wang, E. Xie, X. Li, D.-P. Fan, K. Song, D. Liang, T. Lu, P. Luo, and L. Shao, “Pvt v2: Improved baselines with pyramid vision transformer,” *CVMMJ*, vol. 8, no. 3, pp. 415–424, 2022.
- [179] Z. Liu, Y. Lin, Y. Cao, H. Hu, Y. Wei, Z. Zhang, S. Lin, and B. Guo, “Swin transformer: Hierarchical vision transformer using shifted windows,” in *ICCV*, 2021.
- [180] D.-P. Fan, M.-M. Cheng, Y. Liu, T. Li, and A. Borji, “Structure-measure: A new way to evaluate foreground maps,” in *ICCV*, 2017.
- [181] M.-M. Cheng and D.-P. Fan, “Structure-measure: A new way to evaluate foreground maps,” *IJCV*, vol. 129, no. 9, pp. 2622–2638, 2021.
- [182] J. Qi, Y. Gao, Y. Hu, X. Wang, X. Liu, X. Bai, S. Belongie, A. Yuille, P. H. Torr, and S. Bai, “Occluded video instance segmentation: A benchmark,” *IJCV*, vol. 130, no. 8, pp. 2022–2039, 2022.
- [183] M. Wang and W. Deng, “Deep visual domain adaptation: A survey,” *NC*, vol. 312, pp. 135–153, 2018.
- [184] F. Zhuang, Z. Qi, K. Duan, D. Xi, Y. Zhu, H. Zhu, H. Xiong, and Q. He, “A comprehensive survey on transfer learning,” *Proceedings of the IEEE*, vol. 109, no. 1, pp. 43–76, 2020.
- [185] Y. Wang, Q. Yao, J. T. Kwok, and L. M. Ni, “Generalizing from a few examples: A survey on few-shot learning,” *ACM CSUR*, vol. 53, no. 3, pp. 1–34, 2020.
- [186] T. Hospedales, A. Antoniou, P. Micaelli, and A. Storkey, “Meta-learning in neural networks: A survey,” *IEEE TPAMI*, vol. 44, no. 9, pp. 5149–5169, 2021.
- [187] Y. Cao, S. Li, Y. Liu, Z. Yan, Y. Dai, P. S. Yu, and L. Sun, “A comprehensive survey of ai-generated content (aigc): A history of generative ai from gan to chatgpt,” *arXiv preprint arXiv:2303.04226*, 2023.
- [188] I. Goodfellow, J. Pouget-Abadie, M. Mirza, B. Xu, D. Warde-Farley, S. Ozair, A. Courville, and Y. Bengio, “Generative adversarial networks,” *CACM*, vol. 63, no. 11, pp. 139–144, 2020.
- [189] A. Radford, L. Metz, and S. Chintala, “Unsupervised representation learning with deep convolutional generative adversarial networks,” in *ICLR*, 2016.
- [190] T. Karras, T. Aila, S. Laine, and J. Lehtinen, “Progressive growing of gans for improved quality, stability, and variation,” in *ICLR*, 2018.
- [191] R. Rombach, A. Blattmann, D. Lorenz, P. Esser, and B. Ommer, “High-resolution image synthesis with latent diffusion models,” in *CVPR*, 2022.
- [192] L. Zhang and M. Agrawala, “Adding conditional control to text-to-image diffusion models,” *arXiv preprint arXiv:2302.05543*, 2023.
- [193] A. Kirillov, E. Mintun, N. Ravi, H. Mao, C. Rolland, L. Gustafson, T. Xiao, S. Whitehead, A. C. Berg, W.-Y. Lo *et al.*, “Segment anything,” *arXiv preprint arXiv:2304.02643*, 2023.
- [194] G.-P. Ji, D.-P. Fan, P. Xu, M.-M. Cheng, B. Zhou, and L. Van Gool, “Sam struggles in concealed scenes—empirical study on” segment anything,” *arXiv preprint arXiv:2304.06022*, 2023.
- [195] J. Masci, U. Meier, D. Ciresan, J. Schmidhuber, and G. Fricout, “Steel defect classification with max-pooling convolutional neural networks,” in *IJCNN*, 2012.
- [196] A. Malhi and R. X. Gao, “Pca-based feature selection scheme for machine defect classification,” *IEEE TIM*, vol. 53, no. 6, pp. 1517–1525, 2004.
- [197] Q. Luo, X. Fang, J. Su, J. Zhou, B. Zhou, C. Yang, L. Liu, W. Gui, and L. Tian, “Automated visual defect classification for flat steel surface: a survey,” *IEEE TIM*, vol. 69, no. 12, pp. 9329–9349, 2020.
- [198] H. Y. Ngan, G. K. Pang, and N. H. Yung, “Automated fabric defect detection—a review,” *IVC*, vol. 29, no. 7, pp. 442–458, 2011.
- [199] A. Kumar, “Computer-vision-based fabric defect detection: A survey,” *IEEE TIE*, vol. 55, no. 1, pp. 348–363, 2008.
- [200] S. Ghorai, A. Mukherjee, M. Gangadaran, and P. K. Dutta, “Automatic defect detection on hot-rolled flat steel products,” *IEEE TIM*, vol. 62, no. 3, pp. 612–621, 2012.
- [201] P. Bergmann, S. Löwe, M. Fauser, D. Sattlegger, and C. Steger, “Improving unsupervised defect segmentation by applying structural similarity to autoencoders,” in *VISIGRAPP*, 2018.
- [202] D. Tabernik, S. Šela, J. Skvarč, and D. Skočaj, “Segmentation-based deep-learning approach for surface-defect detection,” *JIM*, vol. 31, no. 3, pp. 759–776, 2020.
- [203] D.-M. Tsai, S.-K. S. Fan, and Y.-H. Chou, “Auto-annotated deep segmentation for surface defect detection,” *IEEE TIM*, vol. 70, pp. 1–10, 2021.
- [204] P. Bergmann, K. Batzner, M. Fauser, D. Sattlegger, and C. Steger, “The mvtec anomaly detection dataset: a comprehensive real-world dataset for unsupervised anomaly detection,” *IJCV*, vol. 129, no. 4, pp. 1038–1059, 2021.
- [205] P. Bergmann, M. Fauser, D. Sattlegger, and C. Steger, “Mvtec ad—a comprehensive real-world dataset for unsupervised anomaly detection,” in *CVPR*, 2019.
- [206] K.-C. Song, S.-P. Hu, Y.-H. Yan, and J. Li, “Surface defect detection method using saliency linear scanning morphology for silicon steel strip under oil pollution interference,” *ISIJ International*, vol. 54, no. 11, pp. 2598–2607, 2014.
- [207] Y. Bao, K. Song, J. Liu, Y. Wang, Y. Yan, H. Yu, and X. Li, “Triplet-graph reasoning network for few-shot metal generic surface defect segmentation,” *IEEE TIM*, vol. 70, pp. 1–11, 2021.
- [208] Y. He, K. Song, Q. Meng, and Y. Yan, “An end-to-end steel surface defect detection approach via fusing multiple hierarchical features,” *IEEE TIM*, vol. 69, no. 4, pp. 1493–1504, 2019.
- [209] Y. Shi, L. Cui, Z. Qi, F. Meng, and Z. Chen, “Automatic road crack detection using random structured forests,” *IEEE TITS*, vol. 17, no. 12, pp. 3434–3445, 2016.
- [210] L. Cui, Z. Qi, Z. Chen, F. Meng, and Y. Shi, “Pavement distress detection using random decision forests,” in *ICDS*, 2015.
- [211] Y. Huang, C. Qiu, and K. Yuan, “Surface defect saliency of magnetic tile,” *TVCJ*, vol. 36, no. 1, pp. 85–96, 2020.
- [212] G.-P. Ji, M. Zhuge, D. Gao, D.-P. Fan, C. Sakaridis, and L. V. Gool, “Masked vision-language transformer in fashion,” *MIR*, 2023.